

Vision Transformers: From Semantic Segmentation to Dense Prediction

Li Zhang^{1*}, · Jiachen Lu^{1*}, · Sixiao Zheng^{1*}, · Xinxuan Zhao¹, · Xiatian Zhu², · Yanwei Fu¹, · Tao Xiang², · Jianfeng Feng¹, · Philip H.S. Torr³

1 Introduction

Since the introduction of Vision Transformers (ViTs) to image classification Dosovitskiy et al. (2021), the landscape of visual representation learning has gradually shifted away from CNNs He et al. (2016), Huang et al. (2017), Krizhevsky et al. (2012), Simonyan and Zisserman (2015), Szegedy et al. (2015). Inspired by this phenomenal success, *for the first time* we expand the application of ViTs from image classification Dosovitskiy et al. (2021) to more challenging dense prediction (*e.g.*, semantic segmentation). Specifically, we introduce **SEgmentation TTransformer** (SETR) Zheng et al. (2021) to replace the seminal fully convolutional network (FCN) Long et al. (2015) with a ViT for visual representation learning. It is shown that ViT can learn stronger long-range dependency information critical for semantic segmentation in unconstrained scene images Badrinarayanan et al. (2017), Yang et al. (2018), achieving superior semantic segmentation performances. Conceptually, this presents a *sequence-to-sequence* learning perspective, capable of learning discriminative visual representation at full receptive field per layer across all the image patches. Subject to the computational budget, the resolution of convolutional feature maps of a FCN instead needs to reduce progressively, in order to learn more abstract and semantic visual concepts by gradually increased receptive fields. Indeed, there are a number of remedies introduced, *e.g.*, manipulating the convolution operation (large kernel sizes Peng et al. (2017), atrous convolutions Chen et al. (2017), Holschneider et al. (1990), and image/feature pyramids Zhao et al. (2017)), integrating attention modules Huang

et al. (2019), Li et al. (2019), Wang et al. (2018), and decomposed attention Wang et al. (2020). Nonetheless, none of these can fully eliminate the limitation of FCN architecture in receptive field. Instead, our reformulation offers an alternative to the dominating FCN design. Crucially, it has been playing a timing, critical role in forming the recent surge of research on contextual visual representation learning Chen et al. (2022), d’Ascoli et al. (2021), Li et al. (2021a), Liu et al. (2021b), Wang et al. (2022).

Specifically, SETR treats an input image as a sequence of *image patches* represented by learned patch embedding, and transforms the sequence with global self-attention modeling for discriminative feature representation learning. Concretely, we first decompose an image into a grid of fixed-sized patches, forming a sequence of patches. With a linear embedding layer applied to the flattened pixel vectors of every patch, we then obtain a sequence of feature embedding vectors as the input to a ViT. Given the learned features from the encoder ViT, a decoder is then used to recover the original image resolution. Crucially there is *no* down-sampling in spatial resolution but global context modeling at every layer of the encoder Transformer, thus offering a completely new perspective to the semantic segmentation problem. Despite its strengths, the basic ViT architecture is less effective for broader dense prediction applications like object detection and instance segmentation. This limitation stems from its absence of a pyramidal structure, its lack of adequate local context processing and its considerable computational demands

To address this aforementioned limitation, in this work a novel **Hierarchical Local-Global** (HLG) Transformers architecture is further introduced. Same as recent ViTs Chen et al. (2022), Chu et al. (2021), d’Ascoli et al. (2021), Li et al. (2021a), Liu et al. (2021b), we also borrow the pyramidal structure from CNNs He et al. (2016), Huang et al. (2017). This adaptation is essential

Corresponding author: Li Zhang

E-mail: lizhangfd@fudan.edu.cn

* These authors contributed equally to this work.

¹ School of Data Science, Fudan University, Shanghai, China

² University of Surrey, Guildford, UK

³ University of Oxford, Oxfordshire, UK

for meeting the requirements of object detection and instance segmentation tasks, which benefit from hierarchical feature processing. Critically, we design a generic HLG Transformer layer characterized by *local attention* within windows and *global-attention* across windows. This configuration effectively compensates for the lack of local context processing in basic ViT models, which is crucial for accurately detecting smaller objects, while still leveraging the global context benefits of the vanilla ViT. The integration of these attention mechanisms enables the creation of a family of HLG Transformers that are not only superior in performance but also cost-effective, especially in lightweight configurations. Beyond semantic segmentation, we therefore further apply the proposed HLG Transformers to image classification and object detection problems, demonstrating the potentials of serving as a versatile ViT backbone.

Our **contributions** with SETR are summarized as follows: **(1)** As an exemplar dense prediction problem, we explore the potentials of self-attention mechanism for visual representation learning, offering an alternative to the dominating FCN design. **(2)** We exploit the ViT framework to implement our image representation learning by image sequentialization. **(3)** To extensively examine our representations, we further introduce three decoder designs at varying complexities. Extensive experiments show that our SETR can learn superior visual representations as compared to different FCNs with and without attention modules, yielding new state of the art on ADE20K (50.28%), Pascal Context (55.83%) and competitive results on Cityscapes. Particularly, our entry was ranked the *first* place in the highly competitive ADE20K test server leaderboard at the submission day.

Our preliminary work SETR Zheng et al. (2021) has been published in CVPR 2021. It is *the very first attempt* of exploring the Transformer for dense prediction tasks (*e.g.*, semantic segmentation) in computer vision. Encouragingly, it has been highly recognized in the community and of great impact to the development of many follow-up works. In this paper, we further extend our preliminary version as below: **(1)** Extending the applications of ViTs from semantic segmentation to general dense prediction tasks (*e.g.*, object detection, instance segmentation and semantic segmentation); **(2)** Enhancing the conventional ViT architecture with building block of the new HLG Transformer layer to allow more cost-effective and pyramidal visual representation learning; **(3)** More extensive comparisons with recent stronger ViT variants on image classification, object detection, and semantic segmentation benchmarks, and demonstrating the superiority of our

HLG Transformers over concurrent state-of-the-art alternatives.

2 Related work

2.1 Semantic Segmentation

Semantic segmentation has been significantly boosted by the development of deep neural networks. By removing fully connected layers, a fully convolutional network (FCN) Long et al. (2015) can achieve pixel-wise predictions. While the predictions of FCN are relatively coarse, several CRF/MRF Chen et al. (2015), Liu et al. (2015), Zheng et al. (2015) based approaches are developed to help refine the coarse predictions. To address the inherent tension between semantics and location Long et al. (2015), coarse and fine layers need to be aggregated for both the encoder and decoder. This leads to different variants of the encoder-decoder structures Badrinarayanan et al. (2017), Noh et al. (2015), Ronneberger et al. (2015) for multi-level feature fusion.

Many recent efforts have been focused on addressing the limited receptive field/context modeling problem in FCN. To enlarge the receptive field, DeepLab Chen et al. (2015) and Dilation Yu and Koltun (2016) introduce the dilated convolution. Alternatively, context modeling is the focus of PSPNet Zhao et al. (2017) and DeepLabV2 Chen et al. (2017). The former proposes the PPM module to obtain different region’s contextual information while the latter develops ASPP module that adopts pyramid dilated convolutions with different dilation rates. Decomposed large kernels Peng et al. (2017) are also utilized for context capturing. Recently, attention based models are popular for capturing long range context information. PSANet Zhao et al. (2018) develops the pointwise spatial attention module for dynamically capturing the long range context. DANet Fu et al. (2019) embeds both spatial attention and channel attention. CCNet Huang et al. (2019) alternatively focuses on economizing the heavy computation budget introduced by full spatial attention. DGMN Zhang et al. (2020) builds a dynamic graph message passing network for scene modeling and it can significantly reduce the computational complexity. Note that all these approaches are still based on FCNs where the feature encoding and extraction part are based on classical ConvNets like VGG Simonyan and Zisserman (2015) and ResNet He et al. (2016). In this work, we alternatively rethink the semantic segmentation task from a different perspective.

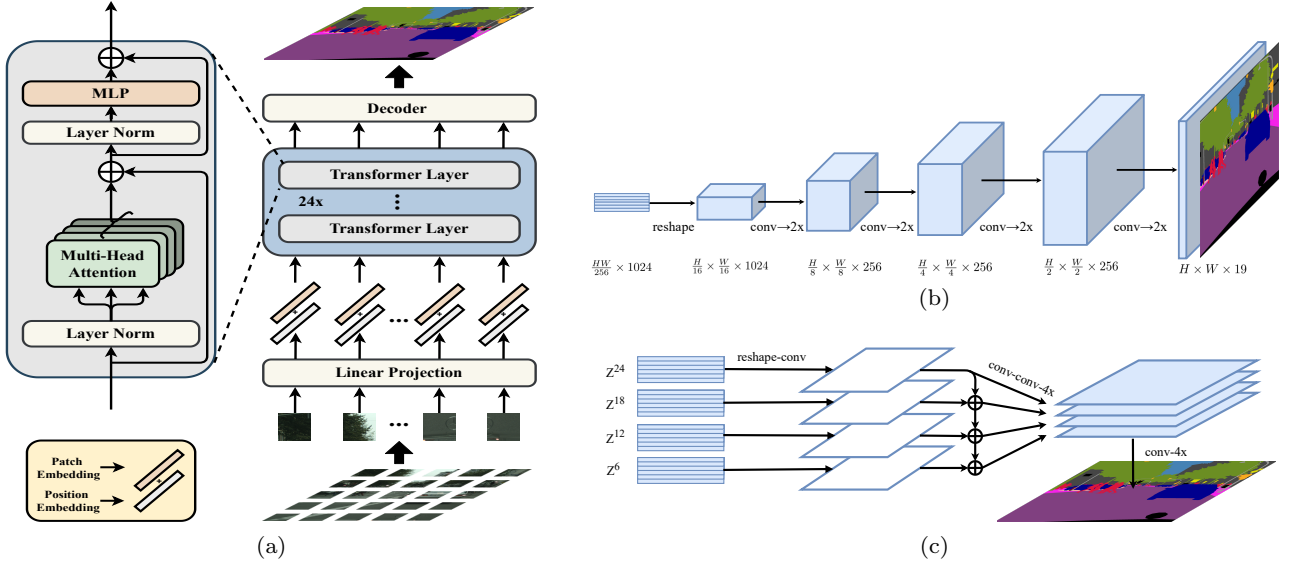


Fig. 1 Schematic illustration of the proposed *Segmentation Transformer (SETR)* (a). We first split an image into fixed-size patches, linearly embed each of them, add position embeddings, and feed the resulting sequence of vectors to a standard Transformer encoder. To perform pixel-wise segmentation, we introduce different decoder designs: (b) progressive upsampling (resulting in a variant called *SETR-PUP*); and (c) multi-level feature aggregation (a variant called *SETR-MLA*).

2.2 Vision Transformers

Transformers have revolutionized machine translation and NLP Dai et al. (2019), Devlin et al. (2019), Vaswani et al. (2017), Yang et al. (2019). Recently, there are also some explorations for the usage of Transformer structures in image recognition. Non-local network Wang et al. (2018) appends Transformer style attention onto the convolutional backbone. AANet Bello et al. (2019) mixes convolution and self-attention for backbone training. LRNet Hu et al. (2019) and stand-alone networks Ramachandran et al. (2019) explore local self-attention to avoid the heavy computation brought by global self-attention. SAN Zhao et al. (2020) explores two types of self-attention modules. Axial-Attention Wang et al. (2020) decomposes the global spatial attention into two separate axial attentions such that the computation is largely reduced. Apart from these pure Transformer based models, there are also CNN-Transformer hybrid ones. DETR Carion et al. (2020) and the following deformable version utilize Transformer for object detection where Transformer is appended inside the detection head. STTR Li et al. (2021b) and LSTR Liu et al. (2021a) adopt Transformer for disparity estimation and lane shape prediction respectively. Recently, ViT Dosovitskiy et al. (2021) is the first work to show that a pure Transformer based image classification model can achieve the state-of-the-art. It provides direct inspiration to exploit Transformer based encoder design for semantic segmentation.

The most related work is Wang et al. (2020) which also leverages attention for image segmentation. However, there are several key differences. First, though convolution is completely removed in Wang et al. (2020) as in our SETR, their model still follows the conventional FCN design in that spatial resolution of feature maps is reduced progressively. In contrast, our prediction model keeps the same spatial resolution throughout and thus represents a step-change in model design. Second, to maximize the scalability on modern hardware accelerators and facilitate easy-to-use, we stick to the standard self-attention design. Instead, Wang et al. (2020) adopts a specially designed axial-attention Ho et al. (2019) which is less scalable to standard computing facilities. Our model is also superior in segmentation accuracy (see Section 4).

Despite the success of ViTs Dosovitskiy et al. (2021) in coarse classification tasks, there is a need for more cost-effective variants and the integration of local and global context relationships for more challenging dense prediction tasks. For example, Transformer in transformer Han et al. (2021) first introduce Transformer block to local patch, but it's still kept in single-stage manner. PVT Wang et al. (2021) first introduces spatial reduction attention in a pyramid architecture. CvT Wu et al. (2021) similarly coalesces ViTs with convolutional inductive bias. CrossViT Chen et al. (2021) instead leverages interaction between large-patch and small-patch branches. Swin Liu et al. (2021b) shifts the local attention windows to capture global cross-window

connection across layers. Rather than employing pure local attention, DiNAT Hassani et al. (2023) applies dilation to local attention and utilizes different dilation rates to achieve global context learning. Recently, (Chu et al., 2021, Li et al., 2022, Song et al., 2022) have directly integrated local and global attention in their attention mechanisms. Local-Global Li et al. (2022) incorporates local attention windows at three different levels. Twins Chu et al. (2021) combines locally-grouped attention with globally sub-sampled attention across the group. GLAM Song et al. (2022) employs channel-wise attention, although it still retains the costly globally self-attention.

While the local attention in these methods remains confined to small windows, which can limit the capture of long-range context, our Hierarchical-Local-Global Transformers utilize dilation in the local windows. This hierarchical approach enables the model to capture both local and long-range information across multiple layers.

3 Method

3.1 FCN-based Semantic Segmentation

In order to contrast with our new model design, let us first revisit the conventional FCN Long et al. (2015) for image semantic segmentation. An FCN encoder consists of a stack of sequentially connected convolutional layers. The first layer takes as input the image, denoted as $H \times W \times 3$ with $H \times W$ specifying the image size in pixels. The input of subsequent layer i is a three-dimensional tensor sized $h \times w \times d$, where h and w are spatial dimensions of feature maps, and d is the feature/channel dimension. Locations of the tensor in a higher layer are computed based on the locations of tensors of all lower layers they are connected to via layer-by-layer convolutions, which are defined as their *receptive fields*. Due to the locality nature of convolution operation, the receptive field increases linearly along the depth of layers, conditional on the kernel sizes (typically 3×3). As a result, only higher layers with big receptive fields can model long-range dependencies in this FCN architecture. However, it is shown that the benefits of adding more layers would diminish rapidly once reaching certain depths He et al. (2016). Having limited receptive fields for context modeling is thus an intrinsic limitation of the vanilla FCN architecture.

Recently, a number of state-of-the-art methods Huang et al. (2019), Zhang et al. (2019, 2020) suggest that combining FCN with attention mechanism is a more effective strategy for learning long-range contextual information. These methods limit the attention learning

to higher layers with smaller input sizes alone due to its quadratic complexity *w.r.t.* the pixel number of feature tensors. This means that dependency learning on lower-level feature tensors is lacking, leading to sub-optimal representation learning. To overcome this limitation, we propose a pure self-attention based encoder, named *SEgmentation TRansformers* (SETR).

3.2 Segmentation Transformers (SETR)

Single-stage Transformer Given the 1D embedding sequence E as input, a pure transformer based encoder is employed to learn feature representations. Concretely, the Transformer, as depicted in Figure 1(a), accepts a 1D sequence of feature embeddings $Z \in \mathbb{R}^{L \times C}$ as input, L is the length of sequence, C is the hidden channel size. This means each transformer layer has a global receptive field, solving the limited receptive field problem of existing FCN encoder once and for all. The transformer encoder consists of L_e layers of multi-head self-attention (MSA) and Multilayer Perceptron (MLP) blocks Velićković et al. (2018) (Figure 1(a)). At each layer l , the input to self-attention is in a triplet of (**query**, **key**, **value**) computed from the input $Z^{l-1} \in \mathbb{R}^{L \times C}$ as:

$$\text{query} = Z^{l-1} \mathbf{W}_Q, \text{key} = Z^{l-1} \mathbf{W}_K, \text{value} = Z^{l-1} \mathbf{W}_V, \quad (1)$$

where $\mathbf{W}_Q/\mathbf{W}_K/\mathbf{W}_V \in \mathbb{R}^{C \times d}$ are the learnable parameters of three linear projection layers and d is the dimension of (**query**, **key**, **value**). Self-attention (SA) is then formulated as:

$$SA(Z^{l-1}) = Z^{l-1} + \text{softmax}\left(\frac{Z^{l-1} \mathbf{w}_Q (Z^{l-1} \mathbf{w}_K)^\top}{\sqrt{d}}\right) (Z^{l-1} \mathbf{w}_V). \quad (2)$$

MSA is an extension with m independent SA operations and project their concatenated outputs: $MSA(Z^{l-1}) = [SA_1(Z^{l-1}); SA_2(Z^{l-1}); \dots; SA_m(Z^{l-1})] \mathbf{W}_O$, where $\mathbf{W}_O \in \mathbb{R}^{md \times C}$. d is typically set to C/m . The output of MSA is then transformed by an MLP block with residual skip as the layer output as:

$$Z^l = MSA(Z^{l-1}) + MLP(MSA(Z^{l-1})) \in \mathbb{R}^{L \times C}. \quad (3)$$

Note, layer norm is applied before MSA and MLP blocks which is omitted for simplicity. We denote $\{Z^1, Z^2, \dots, Z^{L_e}\}$ as the features of transformer layers.

Image to sequence To suit the 1D embedding sequence as input, there thus exists a mismatch between 2D image and 1D sequence. Image sequentialization is thus needed to convert an input image $x \in \mathbb{R}^{H \times W \times 3}$ into Z .

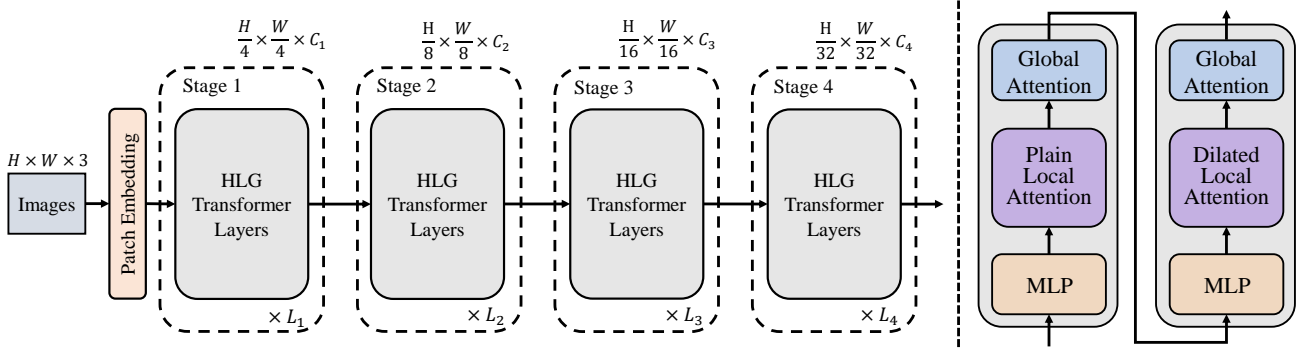


Fig. 2 Left: Hierarchical local-global Transformers backbone architecture. **Right:** Successive hierarchical local-global Transformer layer.

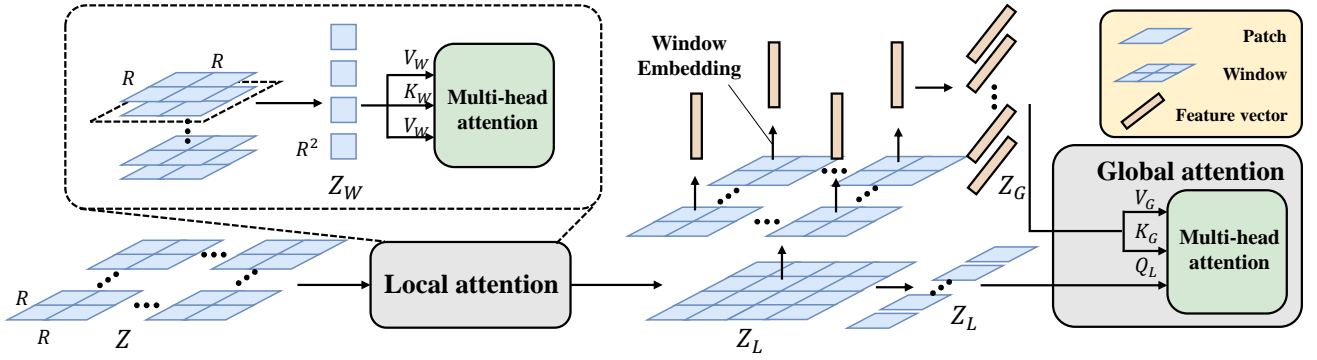


Fig. 3 Local-Global attention mechanism. Local attention (in dash line) is applied within each window. Global attention is applied between global feature Z_G and local feature Z_L .

A straightforward way for image sequentialization is to flatten the image pixel values into a 1D vector with size of $3HW$. For a typical image sized at $480(H) \times 480(W) \times 3$, the resulting vector will have a length of 691,200. Given the quadratic model complexity of Transformer, it is not possible that such high-dimensional vectors can be handled in both space and time. Therefore tokenizing every single pixel as input to our transformer is out of the question.

In view of the fact that a typical encoder designed for semantic segmentation would downsample a 2D image $x \in \mathbb{R}^{H \times W \times 3}$ into a feature map $x_f \in \mathbb{R}^{\frac{H}{16} \times \frac{W}{16} \times C}$, we thus decide to set the transformer input sequence length L as $\frac{H}{16} \times \frac{W}{16} = \frac{HW}{256}$. This way, the output sequence of the transformer can be simply reshaped to the target feature map x_f .

To obtain the $\frac{HW}{256}$ -long input sequence, we divide an image $x \in \mathbb{R}^{H \times W \times 3}$ into a grid of $\frac{H}{16} \times \frac{W}{16}$ patches uniformly, and then flatten this grid into a sequence. By further mapping each vectorized patch p into a latent C -dimensional embedding space using a linear projection function $f: p \rightarrow e \in \mathbb{R}^C$, we obtain a 1D sequence of patch embeddings for an image x . To encode the patch spacial information, we learn a specific embedding p_i

for every location i which is added to e_i to form the final sequence input $E = \{e_1 + p_1, e_2 + p_2, \dots, e_L + p_L\}$. This way, spatial information is kept despite the orderless self-attention nature of transformers.

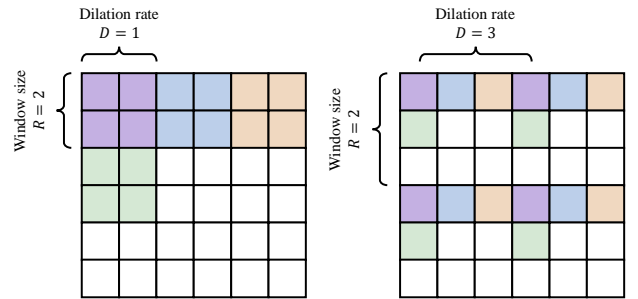


Fig. 4 Left: plain local attention; **Right:** dilated local attention.

3.3 Hierarchical Local-Global Transformer

As a conventional ViT Dosovitskiy et al. (2021) learns feature representation of a single resolution with quadratic computation complexity *w.r.t* the input image size, it is not appropriate to be a backbone network to support various fine downstream tasks, *e.g.*, object detection and instance segmentation. In this paper, we introduce a family of **Hierarchical Local-Global** (HLG) Transformers in a pyramidal structure, serving as a general-purpose backbone network. An overview of our HLG architecture is depicted in Figure 2. A HLG model consists of four stages for multi-scale feature representation learning. Specifically, an input image is first fed to the patch embedding module and downsampled by overlapping patch divisions, followed by L_i HLG layers with i the stage index. All stages share the same structure including one patch embedding module and multiple encoding modules. The output size of each stage $x_f^0, x_f^1, x_f^2, x_f^3$ is designated to be $\frac{H}{4} \times \frac{W}{4}, \frac{H}{8} \times \frac{W}{8}, \frac{H}{16} \times \frac{W}{16}, \frac{H}{32} \times \frac{W}{32}$ sequentially. Next, we describe the key design of the proposed HLG Transformer layer.

Local-Global attention An illustration of our local-global attention is given at Figure 3.

Local attention Given an input feature map Z of size $N_h \times N_w$, it is first divided into $\frac{N_h \times N_w}{R^2}$ windows in a non-overlapping manner, where $R \times R$ represents the window size. The multi-head self-attention is then applied within each local window $Z_W \in \mathbb{R}^{R \times R \times C}$. The attention operation can be expressed as:

$$Q_W = Z_W \mathbf{W}_Q^{(L)}, K_W = Z_W \mathbf{W}_K^{(L)}, V_W = Z_W \mathbf{W}_V^{(L)} \quad (4)$$

$$\text{SA}(Z_W) = Z_W + \text{softmax} \left(\frac{Q_W K_W^\top}{\sqrt{d}} + B_W \right) V_W, \quad (5)$$

where $\mathbf{W}_Q^{(L)}, \mathbf{W}_K^{(L)}, \mathbf{W}_V^{(L)} \in \mathbb{R}^{C \times d}$ are learnable parameters of three linear projection layers shared by all windows and d is the dimension of Q_W, Q_K, Q_V . $B_W \in \mathbb{R}^{R^2 \times R^2}$ is local relative positional encoding. Then we assemble each window feature back to obtain the local feature map $Z_L \in \mathbb{R}^{N_h \times N_w \times C}$. This *plain local attention* can be achieved by non-overlapping window division with focus on information exchange between spatially adjacent patches (Figure 4 left). This scheme is however limited to short range interaction within each individual window. To enable long range dependency discovery without extra computation cost, we further introduce a *dilated local attention* mechanism for stronger representation learning (Figure 4 right). In particular, we form another type of window by sampling

patches in a spaced manner, *e.g.*, sampling a patch every three positions as illustrated in (Figure 4). This allows to learn a relatively longer range dependency using efficient local attention.

Global attention Following local feature map Z_L , we further design an efficient global attention for holistic context learning. To that end, we introduce a *Window Embedding* operation that extracts an 1-dimensional feature vector $\mathbb{R}^{1 \times 1 \times C}$ per window. Window embedding operations can be implemented by depth-wise convolution Chollet (2017), average pooling or max pooling with kernel size and stride equal to the window size. Empirically we find average pooling is generally effective for downstream tasks. More details will be discussed in the experiments. As a result, a *compact* global feature map $Z_G \in \mathbb{R}^{\frac{N_h}{R} \times \frac{N_w}{R} \times C}$ can be obtained. Global attention is then applied to feature map Z_L and Z_G . This enables efficient global attention by querying Z_L towards Z_G formulated as:

$$Q_L = Z_L \mathbf{W}_Q^{(G)}, K_G = Z_G \mathbf{W}_K^{(G)}, V_G = Z_G \mathbf{W}_V^{(G)} \quad (6)$$

$$\text{SA}(Z_L, Z_G) = Z_L + \text{softmax} \left(\frac{Q_L K_G^\top}{\sqrt{d}} + B_G \right) V_G, \quad (7)$$

where $\mathbf{W}_Q^{(G)}, \mathbf{W}_K^{(G)}, \mathbf{W}_V^{(G)} \in \mathbb{R}^{C \times d}$ are learnable parameters of three linear projection layers and d is the dimension of Q_W, Q_K, Q_V . $B_G \in \mathbb{R}^{(N_h \times N_w) \times (\frac{N_h}{R} \times \frac{N_w}{R})}$ is global relative positional encoding.

Parameter and computation sharing For further efficiency, we propose to share the parameters and computation between local and global attention. Concretely, all the parameters of local and global attention are shared as

$$\mathbf{W}_Q^{(L)} = \mathbf{W}_Q^{(G)}, \mathbf{W}_K^{(L)} = \mathbf{W}_K^{(G)}, \mathbf{W}_V^{(L)} = \mathbf{W}_V^{(G)} \quad (8)$$

Computation sharing is non-trivial. To that end, we replace Z_L of Eq. (6) with the output of Eq. (5) as:

$$\begin{aligned} Q_L &= \left(Z_W + \text{softmax} \left(\frac{Q_W K_W^\top}{\sqrt{d}} + B_W \right) V_W \right) \mathbf{W}_Q^{(G)} \\ &= Z_W \mathbf{W}_Q^{(L)} + \text{softmax} \left(\frac{Q_W K_W^\top}{\sqrt{d}} + B_W \right) V_W \mathbf{W}_Q^{(G)} \end{aligned}$$

As a result, we achieve the the first term by reusing Eq. (4), and the second term by a computation-friendly depth-wise convolution as

$$Q_L = Q_W + \text{DWConv}(V_W) \quad (9)$$

where Q_W and K_W are shared with local attention.

DWMLP Following Sandler et al. (2018), Yang et al. (2022), we implement our MLP with a depth-wise convolution and squeeze-and-excitation Hu et al. (2018). We place the MLP before attention so that downsampling can be achieved simply by setting the stride of MLP (first layer in each stage) as 2.

Hierarchical Local-Global Transformer layer To facilitate synergistic interaction without extra complexity and computational cost, we intertwine the plain and dilated local attention sequentially. Both use the same window size. This attention cascading design results in our Hierarchical Local-Global (HLG) Transformer layer (Figure 2 right).

Architecture design

Table 1 summarizes the family of our HLG Transformers with a variety of capacities, including HLG-Mobile, -Tiny, -Small, -Medium, -Large. The hyperparameters are explained as follows:

- C_i : The embedding dimension of each stage i ;
- H_i : The number of head in stage i ;
- R_i : The window size of local attention;
- D_i : The dilation rate of local attention.

3.4 Decoder Designs

Singl-stage Transformer segmentation decoder

To evaluate the effectiveness of SETR’s encoder feature representations Z , we introduce three different decoder designs to perform pixel-level segmentation. As the goal of the decoder is to generate the segmentation results in the original 2D image space ($H \times W$), we need to reshape the encoder’s features (that are used in the decoder), Z , from a 2D shape of $\frac{HW}{256} \times C$ to a standard 3D feature map $\frac{H}{16} \times \frac{W}{16} \times C$. Next, we briefly describe the three decoders.

(1) Naive upsampling (Naive) This naive decoder first projects the transformer feature Z^{L_e} to the dimension of category number (*e.g.*, 19 for experiments on Cityscapes). For this we adopt a simple 2-layer network with architecture: 1×1 conv + sync batch norm (w/ ReLU) + 1×1 conv. After that, we simply bilinearly upsample the output to the full image resolution, followed by a classification layer with pixel-wise cross-entropy loss. When this decoder is used, we denote our model as SETR-*Naïve*.

(2) Progressive UPsampling (PUP) Instead of one-step upscaling which may introduce noisy predictions, we consider a *progressive upsampling* strategy that alternates conv layers and upsampling operations. To maximally mitigate the adversarial effect, we restrict upsampling to $2\times$. Hence, a total of 4 operations are needed for reaching the full resolution from Z^{L_e} with size $\frac{H}{16} \times$

$\frac{W}{16}$. More details of this process are given in Figure 1(b). When using this decoder, we denote our model as SETR-*PUP*.

(3) Multi-Level feature Aggregation (MLA) The third design is characterized by multi-level feature aggregation (Figure 1(c)) in similar spirit of feature pyramid network Kirillov et al. (2019), Lin et al. (2017). However, our decoder is fundamentally different because the feature representations Z^l of every SETR’s layer share the same resolution without a pyramid shape.

Specifically, we take as input the feature representations $\{Z^m\}$ ($m \in \{\frac{L_e}{M}, 2\frac{L_e}{M}, \dots, M\frac{L_e}{M}\}$) from M layers uniformly distributed across the layers with step $\frac{L_e}{M}$ to the decoder. M streams are then deployed, with each focusing on one specific selected layer. In each stream, we first reshape the encoder’s feature Z^l from a 2D shape of $\frac{HW}{256} \times C$ to a 3D feature map $\frac{H}{16} \times \frac{W}{16} \times C$. A 3-layer (kernel size 1×1 , 3×3 , and 3×3) network is applied with the feature channels halved at the first and third layers respectively, and the spatial resolution upscaled $4\times$ by bilinear operation after the third layer. To enhance the interactions across different streams, we introduce a top-down aggregation design via element-wise addition after the first layer. An additional 3×3 conv is applied after the element-wise added feature. After the third layer, we obtain the fused feature from all the streams via channel-wise concatenation which is then bilinearly upsampled $4\times$ to the full resolution. When using this decoder, we denote our model as SETR-*MLA*.

Hierarchical Transformer segmentation decoder

We detail the integration of HLG for segmentation. To align with the input format (*i.e.*, a spatial shape of $\frac{H}{16} \times \frac{W}{16}$) of SETR decoder, we interpolate the features of all four stages to this shape, followed by concatenating and transforming them into a single tensor. The decoder uses a pair of HLG Transformer layers with plain and dilated local attention with the window size R set to 8. The segmentation result is obtained by Progressive UPsampling (PUP).

Hierarchical Transformer decoder In addition to adapting the hierarchical Transformer architecture to single-stage transformers, the pyramidal structure facilitates the use of the same decoders that are common in CNN-based methods. We employ UperNet Xiao et al. (2018a) as the pyramidal segmentation decoder, RetinaNet Lin et al. (2017) for object detection, and MaskRCNN He et al. (2017) as the decoder for instance segmentation.

Table 1 Architecture specifications of HLG. $Conv3 \times 3$ means the convolution with a kernel size of 3×3 , $Conv1 \times 1$ denotes the convolution with a kernel size of 1×1 , and $DWConv3 \times 3$ represents the depth-wise convolution with a kernel size of 3×3 .

Output	HLG-Mobile	HLG-Tiny	HLG-Small	HLG-Medium	HLG-Large
	$Conv3 \times 3(\text{stride} = 2), Conv1 \times 1, Conv3 \times 3(\text{stride} = 2)$				
56×56	$\begin{bmatrix} C_1 = 48 \\ H_1 = 2 \\ R_1 = 7 \\ D_1 = 8 \end{bmatrix} \times 2$	$\begin{bmatrix} C_1 = 64 \\ H_1 = 2 \\ R_1 = 7 \\ D_1 = 8 \end{bmatrix} \times 2$	$\begin{bmatrix} C_1 = 96 \\ H_1 = 3 \\ R_1 = 7 \\ D_1 = 8 \end{bmatrix} \times 2$	$\begin{bmatrix} C_1 = 96 \\ H_1 = 3 \\ R_1 = 7 \\ D_1 = 8 \end{bmatrix} \times 2$	$\begin{bmatrix} C_1 = 128 \\ H_1 = 4 \\ R_1 = 7 \\ D_1 = 8 \end{bmatrix} \times 2$
	$DWConv3 \times 3(\text{stride} = 2)$				
28×28	$\begin{bmatrix} C_2 = 96 \\ H_2 = 4 \\ R_2 = 7 \\ D_2 = 4 \end{bmatrix} \times 2$	$\begin{bmatrix} C_2 = 128 \\ H_2 = 4 \\ R_2 = 7 \\ D_2 = 4 \end{bmatrix} \times 2$	$\begin{bmatrix} C_2 = 192 \\ H_2 = 6 \\ R_2 = 7 \\ D_2 = 4 \end{bmatrix} \times 2$	$\begin{bmatrix} C_2 = 192 \\ H_2 = 6 \\ R_2 = 7 \\ D_2 = 4 \end{bmatrix} \times 2$	$\begin{bmatrix} C_2 = 256 \\ H_2 = 8 \\ R_2 = 7 \\ D_2 = 4 \end{bmatrix} \times 2$
	$DWConv3 \times 3(\text{stride} = 2)$				
14×14	$\begin{bmatrix} C_3 = 192 \\ H_3 = 8 \\ R_3 = 7 \\ D_3 = 2 \end{bmatrix} \times 2$	$\begin{bmatrix} C_3 = 256 \\ H_3 = 8 \\ R_3 = 7 \\ D_3 = 2 \end{bmatrix} \times 6$	$\begin{bmatrix} C_3 = 384 \\ H_3 = 12 \\ R_3 = 7 \\ D_3 = 2 \end{bmatrix} \times 6$	$\begin{bmatrix} C_3 = 384 \\ H_3 = 12 \\ R_3 = 7 \\ D_3 = 2 \end{bmatrix} \times 14$	$\begin{bmatrix} C_3 = 512 \\ H_3 = 16 \\ R_3 = 7 \\ D_3 = 2 \end{bmatrix} \times 14$
	$DWConv3 \times 3(\text{stride} = 2)$				
7×7	$\begin{bmatrix} C_4 = 384 \\ H_4 = 16 \\ R_4 = 7 \\ D_4 = 1 \end{bmatrix} \times 2$	$\begin{bmatrix} C_4 = 512 \\ H_4 = 16 \\ R_4 = 7 \\ D_4 = 1 \end{bmatrix} \times 2$	$\begin{bmatrix} C_4 = 768 \\ H_4 = 24 \\ R_4 = 7 \\ D_4 = 1 \end{bmatrix} \times 2$	$\begin{bmatrix} C_4 = 768 \\ H_4 = 24 \\ R_4 = 7 \\ D_4 = 1 \end{bmatrix} \times 2$	$\begin{bmatrix} C_4 = 1024 \\ H_4 = 32 \\ R_4 = 7 \\ D_4 = 1 \end{bmatrix} \times 2$

Table 2 Configuration of SETR backbone variants.

Model	T-layers	Hidden size	Att head
T-Base	12	768	12
T-Large	24	1024	16

4 Experiments

4.1 Single-stage Transformer Setup

We conduct experiments on three representative semantic segmentation benchmark datasets to evaluate performance on single-stage Transformer.

Semantic segmentation datasets Cityscapes Cordts et al. (2016a) densely annotates 19 object categories in images with urban scenes. It contains 5000 finely annotated images, split into 2975, 500 and 1525 for training, validation and testing respectively. The images are all captured at a high resolution of 2048×1024 . In addition, it provides 19,998 coarse annotated images for model training. **ADE20K Zhou et al. (2019)** is a challenging scene parsing benchmark with 150 fine-grained semantic concepts. It contains 20210, 2000 and 3352 images for training, validation and testing.

Implementation details Following the default setting (*e.g.*, data augmentation and training schedule) of public codebase *mmsegmentation* OpenMMLab (2020), (i) we apply random resize with ratio between 0.5 and 2, random cropping (768, 512 and 480 for Cityscapes and ADE20K respectively) and random horizontal flipping during training for all the experiments; (ii) We set batch size 16 and the total iteration to 160,000 and 80,000 for the experiments on ADE20K. For Cityscapes, we set batch size to 8 with a number of training schedules reported in Table 3, 6 and 9 for fair comparison. We adopt a polynomial learning rate decay schedule Zhao et al. (2017) and employ SGD as the optimizer. Momentum and weight decay are set to 0.9 and 0 respectively for all the experiments on the three datasets. We set initial learning rate 0.001 on ADE20K, and 0.01 on Cityscapes.

Auxiliary loss As Zhao et al. (2017) we also find the auxiliary segmentation loss helps the model training. Each auxiliary loss head follows a 2-layer network. We add auxiliary losses at different Transformer layers: SETR-*Naïve* (Z^{10}, Z^{15}, Z^{20}), SETR-*PUP* ($Z^{10}, Z^{15}, Z^{20}, Z^{24}$), SETR-*MLA* ($Z^6, Z^{12}, Z^{18}, Z^{24}$). Both auxiliary loss and main loss heads are applied concurrently.

Multi-scale test We use the default settings of *mmsegmentation* OpenMMLab (2020). Specifically, the input

Table 3 Comparing SETR variants on different pre-training strategies and backbones. All experiments are trained on Cityscapes train fine set with batch size 8, and evaluated using the single scale test protocol on the Cityscapes validation set in mean IoU (%) rate. “Pre” denotes the pre-training of Transformer part. “R” means the Transformer part is randomly initialized. “w.o.aux” means “without auxiliary loss” and “2step” means 2 upsample layers. The bolded values highlight the best performance in each respective category.

Method	Pretrain	Backbone	#Params	FLOPs	FPS	Mem	40k	80k
FCN OpenMMLab (2020)	1K	R-101	69M	620G	24	1237M	73.93	75.52
Semantic FPN OpenMMLab (2020)	1K	R-101	48M	146G	133	1074M	-	75.80
SETR- <i>Naïve</i>	21K	T-Large	306M	960G	21	3321M	77.37	77.90
SETR- <i>MLA</i>	21K	T-Large	311M	972G	20	3353M	76.65	77.24
SETR-<i>PUP</i>	21K	T-Large	318M	1083G	18	3582M	78.39	79.34
SETR- <i>PUP</i>	R	T-Large	318M	1083G	18	3582M	42.27	-
SETR- <i>Naïve-Base</i>	21K	T-Base	88M	296G	7	1472M	75.54	76.25
SETR- <i>MLA-Base</i>	21K	T-Base	93M	307G	7	1507M	75.60	76.87
SETR-<i>PUP-Base</i>	21K	T-Base	98M	417G	6	1877M	76.71	78.02
SETR- <i>Naïve-DeiT</i>	1K	T-Base	88M	296G	7	1472M	77.85	78.66
SETR- <i>MLA-DeiT</i>	1K	T-Base	93M	307G	7	1507M	78.04	78.98
SETR-<i>PUP-DeiT</i>	1K	T-Base	98M	417G	6	1877M	78.79	79.45
SETR- <i>MLA-BEiT</i>	21K	T-Large	311M	972G	20	3353M	79.59	80.20
SETR-<i>PUP-BEiT</i>	21K	T-Large	318M	1083G	18	3582M	79.84	80.43
SETR- <i>Naïve-w.o.aux</i>	21K	T-Large	306M	960G	21	3321M	76.73	77.23
SETR- <i>PUP-2step</i>	21K	T-Large	308M	990G	18	3455M	77.48	78.58

Table 4 Comparison to FCN with different pre-training with single-scale inference on the ADE20K val and Cityscapes val set. The bolded values highlight the best performance in each respective category.

Method	Pre	Backbone	ADE20K			Cityscapes		
			FLOPs	FPS	mIoU	FLOPs	FPS	mIoU
FCN OpenMMLab (2020)	1K	R-101	276G	111	39.91	620G	24	73.93
FCN	21K	R-101	276G	111	42.17	620G	24	76.38
SETR- <i>MLA</i>	21K	T-Large	368G	80	48.64	972G	7	76.65
SETR- <i>PUP</i>	21K	T-Large	426G	70	48.58	1083G	6	78.39
SETR- <i>MLA-DeiT</i>	1K	T-Base	113G	204	46.15	307G	20	78.98
SETR- <i>PUP-DeiT</i>	1K	T-Base	170G	181	46.24	417G	18	79.45
SETR- <i>MLA-BEiT</i>	21K	T-Large	368G	80	53.0	972G	7	80.20
SETR- <i>PUP-BEiT</i>	21K	T-Large	426G	70	52.5	1083G	6	80.43

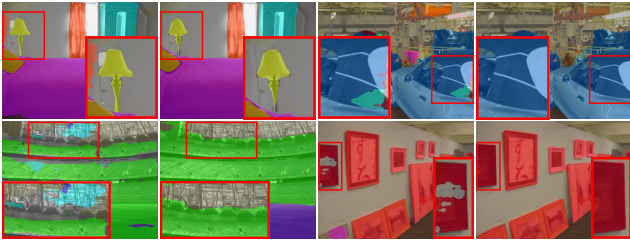


Fig. 5 Qualitative results on ADE20K: SETR (right column) vs. dilated FCN baseline (left column) in each pair. Best viewed in color and zoom in.

image is first scaled to a uniform size. Multi-scale scaling and random horizontal flip are then performed on the image with a scaling factor (0.5, 0.75, 1.0, 1.25, 1.5, 1.75). Sliding window is adopted for test (e.g., 512×512 for ADE20K). If the shorter side is smaller than the

size of the sliding window, the image is scaled with its shorter side to the size of the sliding window (e.g., 512) while keeping the aspect ratio. Synchronized BN is used in decoder and auxiliary loss heads. For training simplicity, we do not adopt the widely-used tricks such as OHEM Yuan and Wang (2018) loss in model training.

Baselines We adopt dilated FCN Long et al. (2015) and Semantic FPN Kirillov et al. (2019) as baselines with their results taken from OpenMMLab (2020). Our models and the baselines are trained and tested in the same settings for fair comparison. In addition, state-of-the-art models are also compared. Note that the dilated FCN is with output stride 8 and we use output stride 16 in all our models due to GPU memory constrain.

SETR variants

Table 5 State-of-the-art comparison on the ADE20K dataset. Performances of different model variants are reported. SS: Single-scale inference. MS: Multi-scale inference. The bolded values highlight the best performance in each respective category.

Method	Pre	Backbone	#Params	Flops	mIoU
FCN (160k, SS) OpenMMLab (2020)	1K	ResNet-101	69M	276G	39.9
FCN (160k, MS) OpenMMLab (2020)	1K	ResNet-101	69M	276G	41.4
PSPNet Zhao et al. (2017)	1K	ResNet-101	68M	256G	44.4
DLabV3+ Chen et al. (2018)	1K	ResNet-101	62M	262G	46.9
CCNet Huang et al. (2019)	1K	ResNet-101	68M	278G	43.7
UperNet Xiao et al. (2018b) (160k, MS)	1K	Swin-T	60M	236G	45.8
UperNet Xiao et al. (2018b) (160k, MS)	1K	Swin-S	81M	259G	49.5
UperNet Xiao et al. (2018b) (160k, MS)	1K	Swin-B	121M	297G	49.7
SETR- <i>Naïve</i> (160k, SS)	21K	ViT-Large	306M	363G	48.1
SETR- <i>Naïve</i> (160k, MS)	21K	ViT-Large	306M	363G	48.8
SETR- <i>PUP</i> (160k, SS)	21K	ViT-Large	318M	426G	48.6
SETR- <i>PUP</i> (160k, MS)	21K	ViT-Large	318M	426G	50.1
SETR- <i>MLA</i> (160k, SS)	21K	ViT-Large	311M	368G	48.6
SETR-<i>MLA</i> (160k, MS)	21K	ViT-Large	311M	368G	50.3
SETR- <i>PUP-BEiT</i> (160k, SS)	21K	ViT-Large	318M	426G	52.5
SETR- <i>PUP-BEiT</i> (160k, MS)	21K	ViT-Large	318M	426G	52.7
SETR- <i>MLA-BEiT</i> (160k, SS)	21K	ViT-Large	311M	318G	53.0
SETR-<i>MLA-BEiT</i> (160k, MS)	21K	ViT-Large	311M	318G	53.1
SETR- <i>PUP-DeiT</i> (160k, SS)	1K	ViT-Base	98M	170G	46.3
SETR- <i>PUP-DeiT</i> (160k, MS)	1K	ViT-Base	98M	170G	47.3
SETR- <i>MLA-DeiT</i> (160k, SS)	1K	ViT-Base	93M	113G	46.2
SETR-<i>MLA-DeiT</i> (160k, MS)	1K	ViT-Base	93M	113G	47.7
SETR- <i>PUP-HLG-small</i> (160k, MS)	1K	HLG-small	37M	243G	47.3
SETR- <i>PUP-HLG-Med</i> (160k, MS)	1K	HLG-Med	61M	269G	49.3
SETR-<i>PUP-HLG-Large</i> (160k, MS)	1K	HLG-Large	100M	294G	49.8

Three variants of our model with different decoder designs (see Sec. 3.4), namely SETR-*Naïve*, SETR-*PUP* and SETR-*MLA*. Besides, we use two variants of the encoder “T-Base” and “T-Large” with 12 and 24 layers respectively (Table 2). Unless otherwise specified, we use “T-Large” as the encoder for SETR-*Naïve*, SETR-*PUP* and SETR-*MLA*. We denote SETR-*Naïve-Base* as the model utilizing “T-Base” in SETR-*Naïve*.

Pre-training We use the pre-trained weights provided by ViT Dosovitskiy et al. (2021), DeiT Touvron et al. (2021) or BEiT Bao et al. (2022) to initialize all the Transformer layers and the input linear projection layer in our model. We denote SETR-*Naïve-DeiT* as the model utilizing DeiT Touvron et al. (2021) pre-training in SETR-*Naïve-Base* and SETR-*PUP-BEiT* as the model model utilizing BEiT Bao et al. (2022) pre-training in SETR-*PUP*. All the layers without pre-training are randomly initialized. For the Transformer part, we use the weights pre-trained by ViT Dosovitskiy et al. (2021), DeiT Touvron et al. (2021), BEiT Bao et al. (2022) or randomly initialized.

We use patch size 16×16 for all the experiments. We perform 2D interpolation on the pre-trained position embeddings, according to their location in the original image for different input size fine-tuning.

Evaluation metric Following the standard evaluation protocol Cordts et al. (2016a), the metric of mean Intersection over Union (mIoU) averaged over all classes is reported. For ADE20K, additionally pixel-wise accuracy is reported following the existing practice.

4.2 HLG Transformer Setup

In this section, we focus on the evaluation of the proposed HLG Transformers. We first evaluate the image classification task using our HLG Transformers as the backbone. For more extensive and task agnostic evaluations, we further test object detection, instance segmentation, and semantic segmentation.

Image classification dataset The ImageNet-1K dataset Russakovsky et al. (2015) contains 1.28 million training images and 50K validation images from 1,000 object categories used for model training and evaluation respectively.

Image classification details

We validate the performance of a HLG Transformer by training on the training set and reporting the Top-1 accuracy on the validation set. For a fair comparison, we follow the setting of Swin Transformer Liu et al. (2021b)

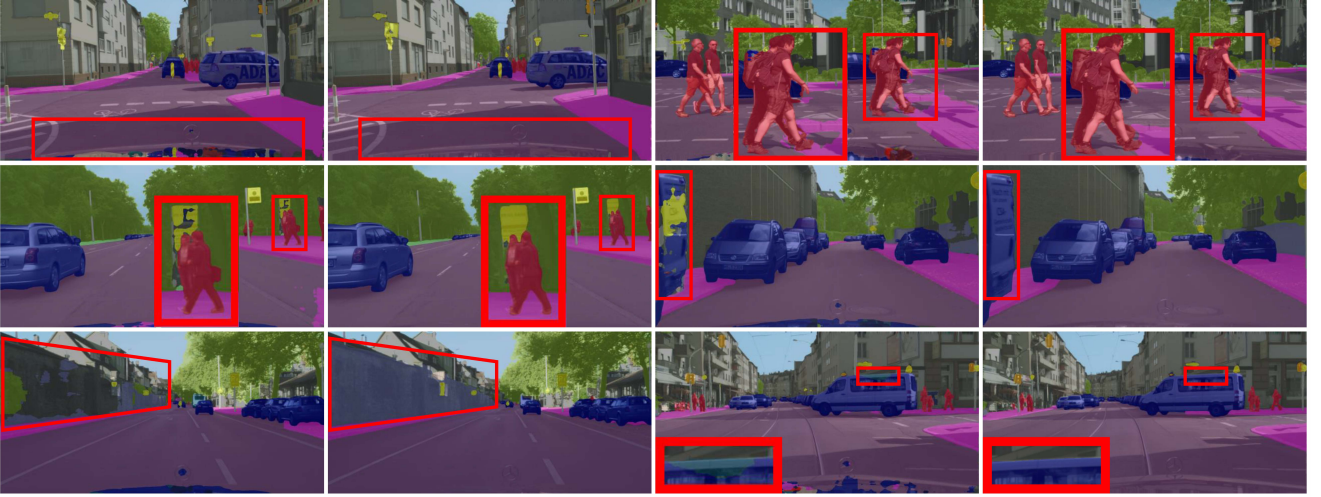


Fig. 6 Qualitative results on Cityscapes: SETR (right column) vs. dilated FCN baseline (left column) in each pair. Best viewed in color and zoom in.

Table 6 State-of-the-art comparison on the Cityscapes validation set. Performances of different training schedules (e.g., 40k and 80k) are reported. SS: Single-scale inference. MS: Multi-scale inference. The bolded values highlight the best performance in each respective category.

Method	Pre	Backbone	#Params	Flops	mIoU
FCN (40k, SS) OpenMMLab (2020)	1K	ResNet-101	68M	619G	73.9
FCN (40k, MS) OpenMMLab (2020)	1K	ResNet-101	68M	619G	75.1
FCN (80k, SS) OpenMMLab (2020)	1K	ResNet-101	68M	619G	75.5
FCN (80k, MS) OpenMMLab (2020)	1K	ResNet-101	68M	619G	76.6
PSPNet Zhao et al. (2017)	1K	ResNet-101	68M	576G	78.5
DLabV3+ Chen et al. (2018)	1K	ResNet-101	62M	571G	79.3
NonLocal Wang et al. (2018)	1K	ResNet-101	66M	669G	79.10
CCNet Huang et al. (2019)	1K	ResNet-101	68M	625G	80.2
GCNet Cao et al. (2019)	1K	ResNet-101	66M	620G	78.1
OCRNet Yuan et al. (2020)	1K	HRNet-W48	70M	972G	81.1
SETR- <i>MLA</i> (80k, MS)	21K	ViT-Large	311M	972G	79.1
SETR-PUP (80k, MS)	21K	ViT-Large	318M	1083G	82.2
SETR- <i>MLA-DeiT</i> (80k, MS)	1K	ViT-Base	93M	307G	78.9
SETR-PUP-DeiT (80k, MS)	1K	ViT-Base	98M	417G	79.5
SETR-PUP-HLG- <i>small</i> (80k, MS)	1K	HLG-small	37M	556G	81.8
SETR-PUP-HLG- <i>Med</i> (80k, MS)	1K	HLG-Med	61M	619G	82.5
SETR-PUP-HLG-Large (80k, MS)	1K	HLG-Large	100M	791G	82.9

and DeiT Touvron et al. (2021). For data augmentation, we perform random-size cropping to 224×224 , and adopt random horizontal flipping Szegedy et al. (2015) and mix up Zhang et al. (2017). Training from scratch, we set the batch size to 1024 and the epochs to 300. We use an initialization learning rate of 0.001, a cosine decay learning rate scheduler with 20 epochs of linear warm-up. We employ the AdamW optimizer with a weight decay of 0.05. To prevent model overfitting, the drop-path Larsson et al. (2016) rate is set to 0.1 by default and 0.3 for HLG-Large due to its stronger capacity.

Semantic segmentation details We use the segmentation framework as SETR-PUP. For more extensive test, we also evaluate UperNet Xiao et al. (2018b) as a second framework. Each backbone network is pre-trained on ImageNet-1k. For a fair comparison, we use the same data augmentation and training schedule as the Swin Transformers Liu et al. (2021b). The training images are randomly deformed at a ratio of 0.5~2 with a cropped size of 768×768 for Cityscapes. Random horizontal flip operation is performed during training. The number of training iteration is set to 40K for Cityscapes. The optimizer uses stochastic gradient descent with momentum of 0.9, weight decay of 0 and

batch size of 8. We adopt the poly learning rate adjustment strategy with the initial learning rate 0.01 for Cityscapes. Only single-scale inference introduced is used.

Object detection dataset

For object detection experiments, we use the COCO 2017 dataset with 118K training and 5K validation images Lin et al. (2014).

Object detection details

For object detection and instance segmentation, we take RetinaNet Lin et al. (2017) and Mask R-cnn He et al. (2017) as the detection framework. The backbone (e.g., ResNet and our HLG Transformer) is initialized with the weights pre-trained on the ImageNet-1k dataset, with the rest initialized by Xavier. We follow the common training settings. We set the batch size to 16 with 1x training schedule (i.e., 12 epochs). We use the AdamW optimizer with a weight decay of 1×10^{-4} and initial learning rate of 1×10^{-4} . Multi-scale training is adopted, while the training images are randomly resized to the shorter side not exceeding 800 pixels and the longer side not exceeding 1333 pixels.

4.3 Vision Transformer Pretraining

We initially examine the pretraining of Vision Transformers. Table 7 compares the results of HLG Transformer with current state-of-the-art ViTs on ImageNet-1k and 21k. The first part of the table showcases the pretrained single-stage Vision Transformers: ViT Dosovitskiy et al. (2021), BeiT Bao et al. (2022), and DeiT Touvron et al. (2022) we employ. It’s evident that single-stage vision transformers are heavily reliant on data scale, with a substantial difference observed between 21K and 1K pretrained ViTs.

Therefore, the hierarchical Vision Transformer addresses the computation cost associated with single-stage Vision Transformer pretraining, allowing for the use of less training data while achieving comparable results. For the hierarchical Vision Transformer, we make the following observations. (1) Compared to the DeiT models, our proposed HLG Transformer is clearly superior in both accuracy and efficiency. For example, HLG-Mobile/Large outperforms DeiT-Ti/B by 2.2%/1.6% in accuracy whilst enjoying less parameters and FLOPs. This is attributed to the hierarchical architecture design and our HLG Transformer design. (2) Compared with the PVT models, all HLG variants remain significantly better. For instance, HLG-Tiny with 11.0M parameters achieves 81.1% accuracy in comparison 75.1% by PVT-T at similar size. This validates the superiority of our HLG Transformer building block over PVT’s

linear attention. (3) Compared with the Swin models similarly characterized by local attentive representation learning, our HLG Transformer counterparts are still more effective in most cases. Particularly, in low-consumption regime, HLG-Small with 34.2M parameters achieves 82.3% accuracy, yielding a margin of 1.0% over Swin-T. For larger models, HLG Transformer achieves a better trade-off between accuracy and model size. Swin-B with 88.0M parameters reaches 83.3%, while our HLG-Large achieves 84.1% with 3.8M fewer parameters.

In Table 8 we show the superiority of our models in the trade-off among efficiency, memory and accuracy on ImageNet1K-V2 Recht et al. (2019) matched frequency dataset, without model overfitting.

4.4 Results of Semantic Segmentation

Ablation Studies Table 3 and 4 show ablation studies on (a) different variants of SETR on various training schedules, (b) comparison to FCN OpenMMLab (2020) and Semantic FPN OpenMMLab (2020), (c) pre-training on different data, and (d) comparison to FCN with different pre-training. Unless specified otherwise, all experiments in Table 3 and 4 are trained on Cityscapes train fine set with batch size 8, and evaluated using the single scale test protocol on the Cityscapes validation set in mean IoU (%) rate. Experiments on ADE20K also follow the single scale test protocol. FPS and memory are tested by single GPU during inference.

From Table 3, we can make the following observations: (i) Progressively upsampling the feature maps, SETR-*PUP* achieves the best performance among all the variants on Cityscapes. One possible reason for inferior performance of SETR-*MLA* is that the feature outputs of different Transformer layers do not have the benefits of resolution pyramid as in feature pyramid network (FPN) (see Figure 7). However, SETR-*MLA* performs slightly better than SETR-*PUP*, and much superior to the variant SETR-*Naïve* that upsamples the Transformers output feature by $16\times$ in one-shot, on ADE20K val set (Table 4 and 5). (ii) The variants utilizing "T-Large" (e.g., SETR-*MLA* and SETR-*Naïve*) outperform their "T-Base" counterparts, namely SETR-*MLA-Base* and SETR-*Naïve-Base*, as anticipated. However, employing superior pre-training techniques on "T-Base" such as DeiT Touvron et al. (2022) yields even better performance for these smaller Vision Transformer models on Cityscapes compared to their larger counterparts. This underscores the significant impact of pre-training methods on performance. (iii) Pre-training is critical for our model. Randomly initialized SETR-*PUP* only

Table 7 Vision Transformer pretraining results on the ILSVRC-2012 ImageNet validation dataset. Performances of different model variants are reported. The bolded values highlight the best performance in each respective category.

Method	Image size	#Params	FLOPs	Top1(%)
ViT-Large-1K Dosovitskiy et al. (2021)	384 ²	307M	44.3G	76.5
ViT-Large-21K Dosovitskiy et al. (2021)	384 ²	307M	44.3G	85.2
BeiT-B-21K Bao et al. (2022)	384 ²	307M	44.3G	86.3
DeiT-B-1K Touvron et al. (2022)	384 ²	87M	49.6G	83.1
DeiT-Ti Touvron et al. (2021)	224 ²	5.7M	1.3G	72.2
CrossViT-Ti Chen et al. (2021)	224 ²	6.9M	1.6G	73.4
HLG-Mobile	224 ²	4.3M	0.9G	75.1
PiT-XS Heo et al. (2021)	224 ²	10.6M	1.4G	78.1
ConT-S Yan et al. (2021)	224 ²	10.1M	1.5G	76.5
PVT-T Wang et al. (2021)	224 ²	13.2M	1.9G	75.1
ConViT-Ti+ d’Ascoli et al. (2021)	224 ²	10.0M	2.0G	76.7
ViP-Ti Bai et al. (2021)	224 ²	12.8M	1.7G	79.0
HLG-Tiny	224 ²	11.0M	2.1G	81.1
LocalViT-S Li et al. (2021a)	224 ²	22.4M	4.6G	80.8
ConViT-S d’Ascoli et al. (2021)	224 ²	27.0M	5.4G	81.3
NesT-S Zhang et al. (2021b)	224 ²	17.0M	5.8G	81.5
Swin-T Liu et al. (2021b)	224 ²	29.0M	4.5G	81.3
CoAtNet-0 Dai et al. (2021)	224 ²	25.0M	4.2G	81.6
DeiT III-S Touvron et al. (2022)	224 ²	22.0M	4.6G	81.4
SwinV2-T Liu et al. (2022a)	256 ²	29.0M	4.5G	81.7
ConvNext-T Liu et al. (2022b)	224 ²	29.0M	4.5G	82.1
HLG-Small	224 ²	24.2M	4.7G	82.3
ConT-M Yan et al. (2021)	224 ²	39.6M	6.4G	81.8
Twins-PCPVT-B Chu et al. (2021)	224 ²	43.8M	6.4G	82.7
PVT-M Wang et al. (2021)	224 ²	44.2M	6.7G	81.2
Swin-S Liu et al. (2021b)	224 ²	50.0M	8.7G	83.0
ConvNext-S Liu et al. (2022b)	224 ²	50.0M	8.7G	83.1
CoAtNet-1 Dai et al. (2021)	224 ²	42.0M	8.4G	83.3
SwinV2-S Liu et al. (2022a)	256 ²	50.0M	8.7G	83.6
HLG-Medium	224 ²	43.7M	9.0G	83.6
DeiT-B Touvron et al. (2021)	224 ²	86.6M	17.6G	81.8
PiT-B Heo et al. (2021)	224 ²	73.8M	12.5G	82.0
ConViT-B d’Ascoli et al. (2021)	224 ²	86.0M	17.0G	82.4
Swin-B Liu et al. (2021b)	224 ²	88.0M	15.4G	83.3
DeiT III-B Touvron et al. (2022)	224 ²	86.6M	15.5G	83.8
ConvNext-S Liu et al. (2022b)	224 ²	89.0M	15.4G	83.8
CoAtNet-2 Dai et al. (2021)	224 ²	75.0M	15.7G	84.1
SwinV2-B Liu et al. (2022a)	256 ²	88.0M	15.4G	84.1
HLG-Large	224 ²	84.2M	15.9G	84.1

gives 42.27% mIoU on Cityscapes. Model pre-trained with BEiT Bao et al. (2022) on ImageNet-21K gives the best performance on Cityscapes and ADE20K, surpassing the alternative pre-trained with ViT Dosovitskiy et al. (2021) on ImageNet-21K. Additionally, employing distillation, DeiT Touvron et al. (2022) pretrained on ImageNet-1K and ”T-Base” Vision Transformer perform better than ImageNet-1K pretrained ”T-Large” Vision Transformer on Cityscapes but worse on ADE20K. This indicates that the reliance of ADE20K on dataset scale for pretraining impacts its performance more significantly due to its diverse range of variants and ample datasets. With appropriate pre-training techniques, employing a smaller model and a smaller pretraining

dataset can outperform larger models pre-trained on larger datasets. (iv) To study the power of pre-training and further verify the effectiveness of our proposed approach, we conduct the ablation study on the pre-training strategy. For fair comparison with the FCN baseline, we first pre-train a ResNet-101 on the ImageNet-21k dataset with a classification task and then adopt the pre-trained weights for a dilated FCN training for semantic segmentation on the target dataset (ADE20K or Cityscapes). As shown in Table 4, with ImageNet-21k pre-training the FCN baseline experiences a clear improvement over the variant pre-trained on ImageNet-1k. However, our method outperforms the FCN counterparts by a large margin, verifying that the advantage

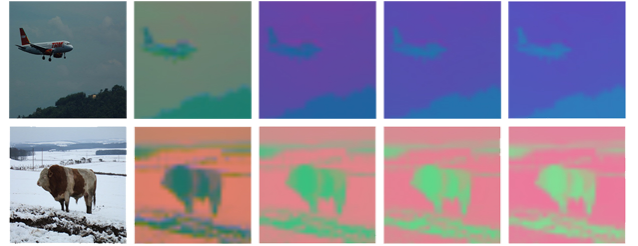
Table 8 Throughput, peak memory and image classification results on ImageNet-1K V2 Recht et al. (2019) matched frequency dataset. The bolded values highlight the best performance in each respective category.

Method	Size	#Params	FLOPs	FPS	Memory	Top1 (%)
Swin-T	224 ²	29M	4.5G	755	11.6GB	69.7
Swin-S	224 ²	50M	8.7G	437	18.6GB	72.1
Swin-B	224 ²	88M	15.4G	278	25.2GB	72.3
HLG-Tiny	224 ²	11M	2.1G	734	11.7GB	70.1
HLG-Small	224 ²	24M	4.7G	697	17.5GB	70.3
HLG-Medium	224 ²	44M	9.0G	392	23.6GB	72.4
HLG-Large	224 ²	84M	15.9G	221	31.6GB	73.2

Table 9 Comparison on the Cityscapes test set. ‡: trained on fine and coarse annotated data. The bolded values highlight the best performance in each respective category.

Method	Backbone	mIoU
PSPNet Zhao et al. (2017)	ResNet-101	78.40
DenseASPP Yang et al. (2018)	DenseNet-161	80.60
BiSeNet Yu et al. (2018)	ResNet-101	78.90
PSANet Zhao et al. (2018)	ResNet-101	80.10
DANet Fu et al. (2019)	ResNet-101	81.50
OCNet Yuan and Wang (2018)	ResNet-101	80.10
CCNet Huang et al. (2019)	ResNet-101	81.90
Axial-DeepLab-L Wang et al. (2020)	Axial-ResNet-L	79.50
Axial-DeepLab-XL Wang et al. (2020)	Axial-ResNet-XL	79.90
SETR- <i>PUP</i> (100k)	T-Large	81.08
SETR-<i>PUP</i>‡	T-Large	81.64

largely comes from the proposed *sequence-to-sequence* representation learning strategy rather than bigger pre-training data. (v) The study on auxiliary loss in Table 3 demonstrates the significant impact of auxiliary loss. It notably enhances model performance, particularly evident at 40,000 iterations. The auxiliary loss aids in regulating the features of the Vision Transformer in early layers, thereby accelerating optimization. (vi) We also investigate the decoder head of SETR-*PUP*. We vary the number of upsample convolution layers from 4 to 2 and adjust the upsampling factor to $4\times$. The results indicate a 0.7% reduction compared to the 4-layer *PUP*. This suggests that maintaining more upsampling layers preserves accuracy during the upsampling operation. (vii) We compare the FLOPS, inference speed, and GPU memory between FCN and different variants of Vision Transformer. As expected, Vision Transformer incurs higher FLOPS, time, and GPU memory usage compared to convolutional models. The increased FLOPS primarily arise from the MLP and self-attention mechanisms in Transformer. Additionally, the larger memory usage mainly stems from the large matrices involved in the scale product of self-attention, which incurs a memory complexity of $\mathcal{O}(n^2)$. Despite the higher computational cost, Vision Transformer boasts overwhelming pretraining scalability. With access to more data and improved pretraining techniques, Vision Transformer

**Fig. 7** Visualization of output feature of layer Z^1 , Z^9 , Z^{17} , Z^{24} of SETR trained on Pascal Context. Best viewed in color.

based segmentation models can achieve superior results compared to the top-performing convolutional models. Moreover, as research advances in higher-performance computation Dao et al. (2022), the cost of Transformers is expected to witness significant optimization.

Results on ADE20K Table 5 presents our results on the challenging ADE20K dataset. Our SETR-*MLA* achieves superior mIoU of 48.64% with single-scale (SS) inference. When multi-scale inference is adopted, our method achieves a new state of the art with mIoU hitting 50.3%. Utilizing the same model, the latest pretraining technique, ViT: BeiT Bao et al. (2022), elevates the SETR to the state of the art with an mIoU of 53.1. Figure 5 shows the qualitative results of our model and dilated FCN on ADE20K. When training a single model on the train+validation set with the default 160,000 iterations,

our method ranks 1st place in the highly competitive ADE20K test server leaderboard.

However, single-stage Transformers suffer from high computational and pretraining costs. Even with DeiT Touvron et al. (2022) to reduce computation costs, the results of SETR paired with DeiT show a significant decline. Thus, we introduce the cost-efficient backbone, Hierarchical Local Global Transformer (HLG). Under similar computational costs, HLG equipped with SETR-PUP achieves the best results in the ImageNet 1K pre-training setting and yields comparable results to SETR-PUP equipped with ViT Large. Additionally, it outperforms the Swin Transformer with UperNet as the decoder head across all parameter levels.

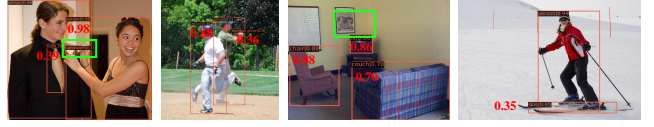
Results on Cityscapes Tables 6 and 9 show the comparative results on the validation and test set of Cityscapes respectively. We can see that our model SETR-PUP is superior to FCN baselines, and FCN plus attention based approaches, such as Non-local Wang et al. (2018) and CCNet Huang et al. (2019); and its performance is on par with the best results reported so far. Similar to the observation in the ADE20K dataset, reducing ViT-Large to ViT-Base results in a significant drop in performance. Therefore, after applying the Hierarchical Local Global Transformer, SETR achieves the best performance with significantly fewer parameters and less computational overhead. Figure 6 shows the qualitative results of our model and dilated FCN on Cityscapes.

4.5 Results of More Dense Prediction Tasks

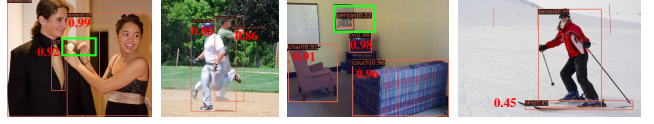
Object Detection

Table 10 shows the bounding box AP results of the RetinaNet detection framework Lin et al. (2017) in different backbones, including both CNNs and ViTs. We have several observations. (1) Compared with top CNNs (*e.g.*, ResNet and ResNeXt), ViTs with the similar parameters can improve the average precision by up to 10.7%. (2) Among ViTs, it is evident that our HLG Transformer achieves the best results across all the size groups. Specifically, compared with PVTv2-B1, HLG-Tiny use a smaller number of parameters to reach a margin of 1.3%. HLG-Large improves over Swin-B and RegionViT-B+ by 3.0% and 1.6% in AP, respectively.

Table 11 reports the bounding box AP and mask box AP of the Mask R-CNN detection framework He et al. (2017) in different backbones. We make similar observations. Our HLG Transformer outperforms all other alternatives consistently. Concretely, HLG-Tiny significantly surpasses ResNet-18 by 7.8%, PVT-Tiny by 4.9%



(a) Detection results of PVT Wang et al. (2021)



(b) Detection results of HLG

Fig. 8 Qualitative object detection results on COCO 2017. The RetinaNet Lin et al. (2017) is used as the framework with (a) PVT-Medium Wang et al. (2021) and (b) HLG-Medium as the backbone in comparison.



(a) Segmentation results of PVT Wang et al. (2021)



(b) Segmentation results of HLG

Fig. 9 Qualitative semantic segmentation results on Cityscapes. The UperNet is used as the framework with (a) PVT-Medium Wang et al. (2021) and (b) HLG-Medium as the backbone in comparison.

and PVT-v2-B1 by 2.9% in AP, using similar parameters. Moreover, HLG-Medium surpasses ResNet-101 by 7.8%, PVT-M by 4.8% and Swin-S by 3.4% using similar parameters. Similar performance margins are achieved by HLG-Small and HLG-Large over the competitors.

Qualitative evaluation

We further provide qualitative evaluation by visualizing the results of object detection and semantic segmentation. We compare our HLG-Medium and PVT-M with similar parameters. For object detection, we use RetinaNet as the framework on COCO. As shown in Figure 8, it is clear that HLG Transformer is superior in detecting small objects, thanks to its ability of better perceiving intra- and inter-patch in visual representation learning. For semantic segmentation, we use the UperNet as the framework on Cityscapes. It is shown in Figure 9 that our HLG Transformer can better segment small object instances. For example, in the first sample, HLG Transformer can infer the segmentation of pedestrians and railings more accurately. In the second sample, the traffic sign can be segmented better by HLG. In the last example, PVT cannot tell apart from

Table 10 Object detection performance using our HLG Transformer with RetinaNet on COCO validation set. The bolded values highlight the best performance in each respective category.

Method	#Params	AP	AP_{50}	AP_{75}	AP_S	AP_M	AP_L
ResNet18 He et al. (2016)	21.3M	31.8	49.6	33.6	16.3	34.3	43.2
PVT-T Wang et al. (2021)	23.0M	36.7	56.9	38.9	22.6	38.8	50.0
PVTv2-B1 Wang et al. (2022)	23.8M	41.2	61.9	43.9	25.4	44.5	54.3
HLG-Tiny	20.7M	43.3	64.4	46.1	28.7	47.6	56.9
ResNet50 He et al. (2016)	37.7M	36.3	55.3	38.6	19.3	40.0	48.8
ConT-M Yan et al. (2021)	27.0M	39.3	59.3	41.8	23.1	43.1	51.9
PVT-S Wang et al. (2021)	34.2M	40.4	61.3	43.0	25.0	42.9	55.7
ViL-S Zhang et al. (2021a)	35.7M	41.6	62.5	44.1	24.9	44.6	56.2
Swin-T Liu et al. (2021b)	38.5M	41.5	62.1	44.2	25.1	44.9	55.5
RegionViT-S+ Chen et al. (2022)	41.6M	43.9	65.5	47.3	28.5	47.3	57.9
HLG-Small	34.4M	44.4	65.6	47.8	30.0	48.6	57.9
ResNet101 He et al. (2016)	56.7M	38.5	57.8	41.2	21.4	42.6	51.1
PVT-M Wang et al. (2021)	53.9M	41.9	63.1	44.3	25.0	44.9	57.6
ViL-M Zhang et al. (2021a)	50.8M	42.9	64.0	45.4	27.0	46.1	57.2
ViP-M Bai et al. (2021)	48.8M	44.3	65.9	47.4	30.7	48.0	57.9
Swin-S Liu et al. (2021b)	59.8M	44.5	65.7	47.5	27.4	48.0	59.9
HLG-Medium	57.9M	46.6	67.9	50.2	31.4	51.0	60.7
ResNeXt101 Xie et al. (2017)	95.5M	41.0	60.9	44.0	23.9	45.2	54.0
PVT-L Wang et al. (2021)	71.1M	42.6	63.7	45.4	25.8	46.0	58.4
ViL-B Zhang et al. (2021a)	66.7M	44.3	65.5	47.1	28.9	47.9	58.3
Swin-B Liu et al. (2021b)	98.4M	44.7	65.9	49.2	-	-	-
RegionViT-B+ Chen et al. (2022)	84.5M	46.1	68.0	49.5	30.5	49.9	60.1
HLG-Large	94.8M	47.7	69.0	51.2	32.8	51.7	62.2

the pedestrians and background around the boundary as well as HLG.

4.6 Ablation studies on HLG

We evaluate two window embedding methods (depth-wise convolution Chollet (2017) and average pooling). For both, we set kernel size and stride as window size. Table 12 shows that the two methods perform similarly on image classification whilst average pooling is better for object detection. One reason is that average pooling can generalize over different kernel sizes flexibly.

Table 13 shows effect of hierarchical local attention mechanism. It is observed that the application of hierarchical local attention mechanism brings 0.64% performance increment.

With PVT as the baseline, Table 14 validates the effect of our key components on ImageNet-1K. Specifically, by adding depth-wise convolution to MLP of Transformer layer and substituting patch embedding with strided depth-wise convolution in MLP, we cut down the parameter size at a cost of slight FLOPs, bringing 1.1% boost. With local attention and sharing parameter/computation over local and global attention, a gain of 1.0% accuracy is obtained with the same parameter size and an admissible FLOPs increment. Hierarchical local attention further yields a gain of 0.4%.

5 Conclusion

In this work, we have presented an alternative perspective for visual representation learning of dense visual prediction tasks by exploiting the ViT architectures. Instead of gradually increasing the receptive field with CNN models, we made a step change at the *architectural* level to elegantly solve the limited receptive field challenge. We implemented the proposed idea with Transformers capable of modeling global context at every stage of representation learning. For tackling general dense visual prediction tasks in a cost-effective manner, we further introduce Hierarchical Local Global (HLG) Transformers with local visual priors and global context learning integrated coherently in a unified architecture. Extensive experiments demonstrate that our models outperform existing alternatives on several visual recognition tasks.

6 Data Availability Statement

The datasets generated during and/or analysed during the current study are available in the Imagenet Rusakovsky et al. (2015) (<https://www.image-net.org/>), ImageNet-v2 Recht et al. (2019) (<https://github.com/modestyachts/ImageNetV2>), COCO Lin et al. (2014) (<https://cocodataset.org>), ADE20K Zhou et al. (2019)

Table 11 Instance segmentation performance using our HLG Transformer with Mask R-CNN on COCO validation set. AP^b denotes bounding box AP and AP^m denotes mask AP. The bolded values highlight the best performance in each respective category.

Method	#Params	AP^b	AP^b_{50}	AP^b_{75}	AP^m	AP^m_{50}	AP^m_{75}
ResNet18 He et al. (2016)	31.2M	36.9	57.1	40.0	33.6	53.9	35.7
PVT-T Wang et al. (2021)	32.9M	39.8	62.2	43.0	37.4	59.3	39.9
PVTv2-B1 Wang et al. (2022)	33.7M	41.8	64.3	45.9	38.8	61.2	41.6
HLG-Tiny	30.6M	44.7	67.1	48.8	40.9	63.7	44.2
ResNet50 He et al. (2016)	44.2M	38.0	58.6	41.4	34.4	55.1	36.7
PVT-S Wang et al. (2021)	44.1M	40.4	62.9	43.8	37.8	60.1	40.3
ViL-S Zhang et al. (2021a)	45.0M	41.8	64.1	45.1	38.5	61.1	41.4
Swin-T Liu et al. (2021b)	47.8M	42.2	64.6	46.2	39.1	61.6	42.0
RegionViT-S+ Chen et al. (2022)	50.9M	44.2	67.3	48.2	40.8	64.1	44.0
HLG-Small	43.7M	46.0	68.6	50.7	42.0	65.7	45.1
ResNet101 He et al. (2016)	63.2M	40.4	61.1	44.2	36.4	57.7	38.8
ResNeXt101 Xie et al. (2017)	62.8M	41.9	62.5	45.9	37.5	59.4	40.2
PVT-M Wang et al. (2021)	63.9M	42.0	64.4	45.6	39.0	61.6	42.1
ViL-M Zhang et al. (2021a)	60.1M	43.4	65.9	47.0	39.7	62.8	42.1
Swin-S Liu et al. (2021b)	69.1M	44.8	66.6	48.9	40.9	63.4	44.2
HLG-Medium	67.3M	48.2	70.2	53.0	43.4	67.0	46.7
ResNeXt101 Xie et al. (2017)	101.9M	42.8	63.8	47.3	38.4	60.6	41.3
PVT-L Wang et al. (2021)	81.0M	42.9	65.0	46.6	39.5	61.9	42.5
ViL-B Zhang et al. (2021a)	76.1M	45.1	67.2	49.3	41.0	64.3	44.2
Swin-B Liu et al. (2021b)	107.2M	45.5	-	-	41.3	-	-
RegionViT-B+ Chen et al. (2022)	93.2M	46.3	69.1	51.2	42.4	66.2	45.6
HLG-Large	103.6M	49.1	71.0	53.9	44.2	68.0	47.8

Table 12 Ablation on window embedding: Performance on ImageNet classification and COCO object detection under different window embedding approaches. “W.E.” means window embedding, “DWConv” means depth-wise convolution Chollet (2017)

Method	W.E.	#Params	Top-1 (%)	AP
HLG-Tiny	DWConv	11.0M	81.14	39.6
HLG-Tiny	Avgpool	11.0M	81.11	42.4

Table 13 Ablation on dilated local distance attention mechanism: Performance on ImageNet classification under different local attention setting. “Plain+plain” denotes that only plain local attention are used in HLG transformer layers while “plain+dila” denotes that plain and dilated local attention are hierarchically applied. The number after “plain+dila” denotes the dilation rate. “W.E.” means window embedding, while “DWConv” means depth-wise convolution Chollet (2017).

Method	W.E.	Hierarchical	#Params	Top-1 (%)
HLG-Tiny	Avgpool	plain+plain	11.0M	80.58
HLG-Tiny	Avgpool	plain+dila 7	11.0M	81.11
HLG-Tiny	Avgpool	plain+dila 5	11.0M	80.77
HLG-Tiny	Avgpool	plain+dila 8	11.0M	81.08

(<https://groups.csail.mit.edu/vision/datasets/ADE20K/>), Cityscapes Cordts et al. (2016b) (<https://www.cityscapes-dataset.com>), Pascal Context Mot-

Table 14 Step by step ablation study. We use PVT Wang et al. (2021) as the baseline but use our architecture specification in Table 1. Term “shared local” denotes shared local attention and “plain+dilated” denotes the plain and dilated local attention are hierarchically applied.

Method	#Params	FLOPs	FPS	Top-1 (%)
Baseline	24.5M	4.0G	802	79.2
+ DWMLP	24.2M	4.2G	793	80.3
++ shared local	24.2M	4.7G	697	81.9
+++ plain+dilated	24.2M	4.7G	697	82.3

taghi et al. (2014) (<https://cs.stanford.edu/~roozbeh/pascal-context/>) repositories.

Acknowledgments

We thank Hengshuang Zhao, Zekun Luo and Yabiao Wang for valuable discussions. This work was supported in part by STI2030-Major Projects (Grant No. 2021ZD0200204), National Natural Science Foundation of China (Grant No. 62106050 and 62376060), Natural Science Foundation of Shanghai (Grant No. 22ZR1407500), USyd-Fudan BISA Flagship Research Program and Lingang Laboratory (Grant No. LG-QS-202202-07).

A Visualizations

A.1 Position Embedding

Visualization of the learned position embedding in Figure 10 shows that the model learns to encode distance within the image in the similarity of position embeddings.

A.2 Features

Figure 12 shows the feature visualization of our SETR-*PUP*. For the encoder, 24 output features from the 24 Transformer layers namely $Z^1 - Z^{24}$ are collected. Meanwhile, 5 features ($U^1 - U^5$) right after each bilinear interpolation in the decoder head are visited.

A.3 Attention Maps

Attention maps (Figure 13 and Figure 14) in each Transformer layer catch our interest. There are 16 heads and 24 layers in T-large. Similar to Abnar and Zuidema (2020), a recursion perspective into this problem is applied. Figure 11 shows the attention maps of different selected spatial points (red).

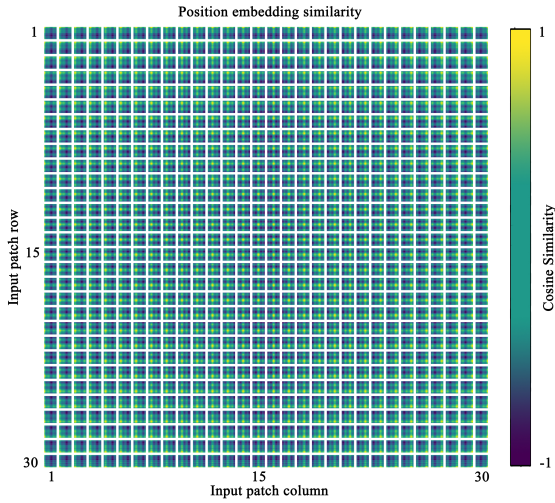


Fig. 10 Similarity of position embeddings of SETR-*PUP* trained on Pascal Context. Tiles show the cosine similarity between the position embedding of the patch with the indicated row and column and the position embeddings of all other patches.

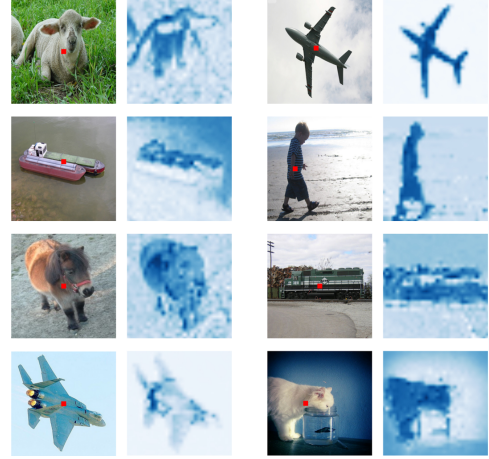


Fig. 11 The first and third columns show images from Pascal Context. The second and fourth columns illustrate the attention map of the picked points (red).



Fig. 12 Visualization of output feature of layer $Z^1 - Z^{24}$ and $U^1 - U^5$ of SETR-*PUP* trained on Pascal Context. Best view in color. **First row:** The input image. **Second row:** Layer $Z^1 - Z^{12}$. **Third row:** Layer $Z^{13} - Z^{24}$. **Fourth row:** Layer $U^1 - U^5$.

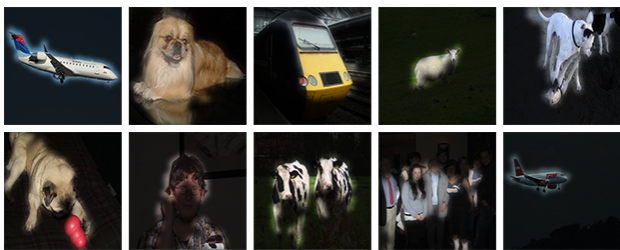


Fig. 13 Examples of attention maps from SETR trained on Pascal Context.

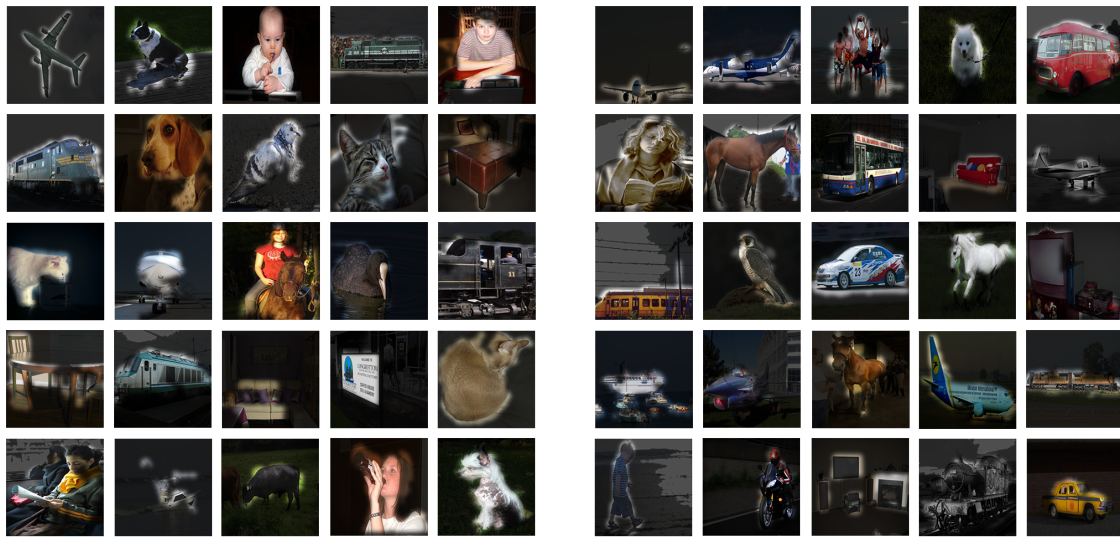


Fig. 14 More examples of attention maps from SETR-*PUP* trained on Pascal Context.

References

- Abnar S, Zuidema W (2020) Quantifying attention flow in transformers. In: Annual Meeting of the Association for Computational Linguistics, pp 4190–4197
- Badrinarayanan V, Kendall A, Cipolla R (2017) Segnet: A deep convolutional encoder-decoder architecture for image segmentation. *IEEE Transactions on Pattern Analysis and Machine Intelligence* 39(12):2481–2495
- Bai S, Torr P, et al. (2021) Visual parser: Representing part-whole hierarchies with transformers. *arXiv preprint*
- Bao H, Dong L, Piao S, Wei F (2022) Beit: Bert pre-training of image transformers. In: International Conference on Learning Representations
- Bello I, Zoph B, Vaswani A, Shlens J, Le QV (2019) Attention augmented convolutional networks. In: *IEEE International Conference on Computer Vision*, pp 10076–10085
- Cao Y, Xu J, Lin S, Wei F, Hu H (2019) Gcnet: Non-local networks meet squeeze-excitation networks and beyond. In: *IEEE International Conference on Computer Vision workshops*, pp 0–0
- Carion N, Massa F, Synnaeve G, Usunier N, Kirillov A, Zagoruyko S (2020) End-to-end object detection with transformers. In: *European Conference on Computer Vision*, pp 213–229
- Chen CF, Panda R, Fan Q (2022) Regionvit: Regional-to-local attention for vision transformers. In: *International Conference on Learning Representations*
- Chen CFR, Fan Q, Panda R (2021) Crossvit: Cross-attention multi-scale vision transformer for image classification. In: *IEEE International Conference on Computer Vision*, pp 357–366
- Chen L, Papandreou G, Kokkinos I, Murphy K, Yuille AL (2015) Semantic image segmentation with deep convolutional nets and fully connected CRFs. In: *International Conference on Learning Representations*
- Chen LC, Papandreou G, Kokkinos I, Murphy K, Yuille AL (2015) Semantic image segmentation with deep convolutional nets and fully connected CRFs. In: *International Conference on Learning Representations*
- Chen LC, Papandreou G, Kokkinos I, Murphy K, Yuille AL (2017) Deeplab: Semantic image segmentation with deep convolutional nets, atrous convolution, and fully connected crfs. *IEEE Transactions on Pattern Analysis and Machine Intelligence* 40(4):834–848
- Chen LC, Zhu Y, Papandreou G, Schroff F, Adam H (2018) Encoder-decoder with atrous separable convolution for semantic image segmentation. In: *European Conference on Computer Vision*, pp 801–818
- Chollet F (2017) Xception: Deep learning with depth-wise separable convolutions. In: *IEEE Conference on Computer Vision and Pattern Recognition*, pp 1251–1258
- Chu X, Tian Z, Wang Y, Zhang B, Ren H, Wei X, Xia H, Shen C (2021) Twins: Revisiting the design of spatial attention in vision transformers. In: *Advances in Neural Information Processing Systems*, pp 9355–9366
- Cordts M, Omran M, Ramos S, Rehfeld T, Enzweiler M, Benenson R, Franke U, Roth S, Schiele B (2016a) The cityscapes dataset for semantic urban scene understanding. In: *IEEE Conference on Computer Vision and Pattern Recognition*, pp 3213–3223
- Cordts M, Omran M, Ramos S, Rehfeld T, Enzweiler M, Benenson R, Franke U, Roth S, Schiele B (2016b) The cityscapes dataset for semantic urban scene understanding. In: *IEEE Conference on Computer Vision and Pattern Recognition*, pp 3213–3223
- Dai Z, Yang Z, Yang Y, Carbonell J, Le QV, Salakhutdinov R (2019) Transformer-xl: Attentive language models beyond a fixed-length context. In: *Annual Meeting of the Association for Computational Linguistics*, pp 2978–2988
- Dai Z, Liu H, Le QV, Tan M (2021) Coatnet: Marrying convolution and attention for all data sizes. In: *Advances in Neural Information Processing Systems*, pp 3965–3977
- Dao T, Fu D, Ermon S, Rudra A, Ré C (2022) Flashattention: Fast and memory-efficient exact attention with io-awareness. *Advances in Neural Information Processing Systems* 35:16344–16359
- Devlin J, Chang MW, Lee K, Toutanova K (2019) BERT: Pre-training of deep bidirectional transformers for language understanding. In: *Proceedings of the Conference of the North American Chapter of the Association for Computational Linguistics: Human Language Technologies*, pp 4171–4186
- Dosovitskiy A, Beyer L, Kolesnikov A, Weissenborn D, Zhai X, Unterthiner T, Dehghani M, Minderer M, Heigold G, Gelly S, et al. (2021) An image is worth 16x16 words: Transformers for image recognition at scale. In: *International Conference on Learning Representations*
- d’Ascoli S, Touvron H, Leavitt ML, Morcos AS, Biroli G, Sagun L (2021) Convit: Improving vision transformers with soft convolutional inductive biases. In: *International Conference on Machine Learning*, PMLR, pp 2286–2296
- Fu J, Liu J, Tian H, Fang Z, Lu H (2019) Dual attention network for scene segmentation. In: *IEEE Conference on Computer Vision and Pattern Recognition*, pp 3146–3154

- Han K, Xiao A, Wu E, Guo J, Xu C, Wang Y (2021) Transformer in transformer. *Advances in neural information processing systems* 34:15908–15919
- Hassani A, Walton S, Li J, Li S, Shi H (2023) Neighborhood attention transformer. In: *IEEE Conference on Computer Vision and Pattern Recognition*, pp 6185–6194
- He K, Zhang X, Ren S, Sun J (2016) Deep residual learning for image recognition. In: *IEEE Conference on Computer Vision and Pattern Recognition*, pp 770–778
- He K, Gkioxari G, Dollár P, Girshick R (2017) Mask r-cnn. In: *IEEE International Conference on Computer Vision*, pp 2961–2969
- Heo B, Yun S, Han D, Chun S, Choe J, Oh SJ (2021) Rethinking spatial dimensions of vision transformers. In: *IEEE International Conference on Computer Vision*, pp 11936–11945
- Ho J, Kalchbrenner N, Weissenborn D, Salimans T (2019) Axial attention in multidimensional transformers. *arXiv preprint*
- Holschneider M, Kronland-Martinet R, Morlet J, Tchamitchian P (1990) A real-time algorithm for signal analysis with the help of the wavelet transform. In: *Wavelets: Time-Frequency Methods and Phase Space Proceedings of the International Conference, Marseille, France, December 14–18, 1987*, Springer, pp 286–297
- Hu H, Zhang Z, Xie Z, Lin S (2019) Local relation networks for image recognition. In: *IEEE International Conference on Computer Vision*, pp 3464–3473
- Hu J, Shen L, Sun G (2018) Squeeze-and-excitation networks. In: *IEEE Conference on Computer Vision and Pattern Recognition*, pp 7132–7141
- Huang G, Liu Z, Van Der Maaten L, Weinberger KQ (2017) Densely connected convolutional networks. In: *IEEE Conference on Computer Vision and Pattern Recognition*, pp 4700–4708
- Huang Z, Wang X, Huang L, Huang C, Wei Y, Liu W (2019) Ccnet: Criss-cross attention for semantic segmentation. In: *IEEE International Conference on Computer Vision*, pp 603–612
- Kirillov A, Girshick R, He K, Dollár P (2019) Panoptic feature pyramid networks. In: *IEEE Conference on Computer Vision and Pattern Recognition*, pp 6399–6408
- Krizhevsky A, Sutskever I, Hinton GE (2012) ImageNet classification with deep convolutional neural networks. *Advances in Neural Information Processing Systems* 25
- Larsson G, Maire M, Shakhnarovich G (2016) Fractalnet: Ultra-deep neural networks without residuals. In: *International Conference on Learning Representations*
- Li J, Yan Y, Liao S, Yang X, Shao L (????) Local-to-global self-attention in vision transformers. *arxiv* 2021. *arXiv preprint arXiv:210704735*
- Li X, Zhang L, You A, Yang M, Yang K, Tong Y (2019) Global aggregation then local distribution in fully convolutional networks. In: *British Machine Vision Conference*, p 244
- Li Y, Zhang K, Cao J, Timofte R, Van Gool L (2021a) Localvit: Bringing locality to vision transformers. *arXiv preprint*
- Li Z, Liu X, Drenkow N, Ding A, Creighton FX, Taylor RH, Unberath M (2021b) Revisiting stereo depth estimation from a sequence-to-sequence perspective with transformers. In: *IEEE Conference on Computer Vision and Pattern Recognition*, pp 6197–6206
- Lin TY, Maire M, Belongie S, Hays J, Perona P, Ramanan D, Dollár P, Zitnick CL (2014) Microsoft coco: Common objects in context. In: *European Conference on Computer Vision*, Springer, pp 740–755
- Lin TY, Dollár P, Girshick RB, He K, Hariharan B, Belongie SJ (2017) Feature pyramid networks for object detection. In: *IEEE Conference on Computer Vision and Pattern Recognition*, pp 2117–2125
- Lin TY, Goyal P, Girshick R, He K, Dollar P (2017) Focal loss for dense object detection. In: *IEEE International Conference on Computer Vision*, pp 2980–2988
- Liu R, Yuan Z, Liu T, Xiong Z (2021a) End-to-end lane shape prediction with transformers. In: *IEEE Winter Conference on Applications of Computer Vision*, pp 3694–3702
- Liu Z, Li X, Luo P, Loy CC, Tang X (2015) Semantic image segmentation via deep parsing network. In: *IEEE International Conference on Computer Vision*, pp 1377–1385
- Liu Z, Lin Y, Cao Y, Hu H, Wei Y, Zhang Z, Lin S, Guo B (2021b) Swin transformer: Hierarchical vision transformer using shifted windows. In: *IEEE International Conference on Computer Vision*, pp 10012–10022
- Liu Z, Hu H, Lin Y, Yao Z, Xie Z, Wei Y, Ning J, Cao Y, Zhang Z, Dong L, et al. (2022a) Swin transformer v2: Scaling up capacity and resolution. In: *IEEE Conference on Computer Vision and Pattern Recognition*, pp 12009–12019
- Liu Z, Mao H, Wu CY, Feichtenhofer C, Darrell T, Xie S (2022b) A convnet for the 2020s. In: *IEEE Conference on Computer Vision and Pattern Recognition*, pp 11976–11986
- Long J, Shelhamer E, Darrell T (2015) Fully convolutional networks for semantic segmentation. In: *IEEE Conference on Computer Vision and Pattern Recognition*

- tion, pp 3431–3440
- Mottaghi R, Chen X, Liu X, Cho NG, Lee SW, Fidler S, Urtasun R, Yuille A (2014) The role of context for object detection and semantic segmentation in the wild. In: IEEE Conference on Computer Vision and Pattern Recognition, pp 891–898
- Noh H, Hong S, Han B (2015) Learning deconvolution network for semantic segmentation. In: IEEE International Conference on Computer Vision, pp 1520–1528
- OpenMMLab (2020) mmsegmentation. <https://github.com/open-mmlab/msegmentation>
- Peng C, Zhang X, Yu G, Luo G, Sun J (2017) Large kernel matters—improve semantic segmentation by global convolutional network. In: IEEE Conference on Computer Vision and Pattern Recognition, pp 4353–4361
- Ramachandran P, Parmar N, Vaswani A, Bello I, Levskaya A, Shlens J (2019) Stand-alone self-attention in vision models. In: Advances in Neural Information Processing Systems, pp 68–80
- Recht B, Roelofs R, Schmidt L, Shankar V (2019) Do imagenet classifiers generalize to imagenet? In: International Conference on Machine Learning, PMLR, pp 5389–5400
- Ronneberger O, Fischer P, Brox T (2015) U-net: Convolutional networks for biomedical image segmentation. In: International Conference on Medical Image Computing and Computer Assisted Intervention, Springer, pp 234–241
- Russakovsky O, Deng J, Su H, Krause J, Satheesh S, Ma S, Huang Z, Karpathy A, Khosla A, Bernstein M, et al. (2015) Imagenet large scale visual recognition challenge. *International Journal of Computer Vision* 115:211–252
- Sandler M, Howard A, Zhu M, Zhmoginov A, Chen LC (2018) Mobilenetv2: Inverted residuals and linear bottlenecks. In: IEEE Conference on Computer Vision and Pattern Recognition, pp 4510–4520
- Simonyan K, Zisserman A (2015) Very deep convolutional networks for large-scale image recognition. In: International Conference on Learning Representations
- Song CH, Han HJ, Avrithis Y (2022) All the attention you need: Global-local, spatial-channel attention for image retrieval. In: IEEE Winter Conference on Applications of Computer Vision, pp 2754–2763
- Szegedy C, Liu W, Jia Y, Sermanet P, Reed S, Anguelov D, Erhan D, Vanhoucke V, Rabinovich A (2015) Going deeper with convolutions. In: IEEE Conference on Computer Vision and Pattern Recognition, pp 1–9
- Touvron H, Cord M, Douze M, Massa F, Sablayrolles A, Jégou H (2021) Training data-efficient image transformers & distillation through attention. In: International Conference on Machine Learning, PMLR, pp 10347–10357
- Touvron H, Cord M, Jégou H (2022) Deit iii: Revenge of the vit. In: Computer Vision—ECCV 2022: 17th European Conference, Tel Aviv, Israel, October 23–27, 2022, Proceedings, Part XXIV, Springer, pp 516–533
- Vaswani A, Shazeer N, Parmar N, Uszkoreit J, Jones L, Gomez AN, Kaiser Ł, Polosukhin I (2017) Attention is all you need. In: Advances in Neural Information Processing Systems, pp 5998–6008
- Veličković P, Cucurull G, Casanova A, Romero A, Lio P, Bengio Y (2018) Graph attention networks. In: International Conference on Learning Representations
- Wang H, Zhu Y, Green B, Adam H, Yuille A, Chen LC (2020) Axial-deeplab: Stand-alone axial-attention for panoptic segmentation. In: European Conference on Computer Vision, Springer, pp 108–126
- Wang W, Xie E, Li X, Fan DP, Song K, Liang D, Lu T, Luo P, Shao L (2021) Pyramid vision transformer: A versatile backbone for dense prediction without convolutions. In: IEEE International Conference on Computer Vision, pp 568–578
- Wang W, Xie E, Li X, Fan DP, Song K, Liang D, Lu T, Luo P, Shao L (2022) Pvt v2: Improved baselines with pyramid vision transformer. *Computational Visual Media* 8(3):415–424
- Wang X, Girshick R, Gupta A, He K (2018) Non-local neural networks. In: IEEE Conference on Computer Vision and Pattern Recognition, pp 7794–7803
- Wu H, Xiao B, Codella N, Liu M, Dai X, Yuan L, Zhang L (2021) Cvt: Introducing convolutions to vision transformers. In: IEEE International Conference on Computer Vision, pp 22–31
- Xiao T, Liu Y, Zhou B, Jiang Y, Sun J (2018a) Unified perceptual parsing for scene understanding. In: European Conference on Computer Vision, pp 418–434
- Xiao T, Liu Y, Zhou B, Jiang Y, Sun J (2018b) Unified perceptual parsing for scene understanding. In: European Conference on Computer Vision, pp 418–434
- Xie S, Girshick R, Dollár P, Tu Z, He K (2017) Aggregated residual transformations for deep neural networks. In: IEEE Conference on Computer Vision and Pattern Recognition, pp 1492–1500
- Yan H, Li Z, Li W, Wang C, Wu M, Zhang C (2021) Contnet: Why not use convolution and transformer at the same time? arXiv preprint
- Yang C, Qiao S, Yu Q, Yuan X, Zhu Y, Yuille A, Adam H, Chen LC (2022) Moat: Alternating mobile convolution and attention brings strong vision models.

- In: International Conference on Learning Representations
- Yang M, Yu K, Zhang C, Li Z, Yang K (2018) Denseaspp for semantic segmentation in street scenes. In: IEEE Conference on Computer Vision and Pattern Recognition, pp 3684–3692
- Yang Z, Dai Z, Yang Y, Carbonell J, Salakhutdinov R, Le QV (2019) Xlnet: Generalized autoregressive pretraining for language understanding. In: Advances in Neural Information Processing Systems, pp 5754–5764
- Yu C, Wang J, Peng C, Gao C, Yu G, Sang N (2018) Bisenet: Bilateral segmentation network for real-time semantic segmentation. In: European Conference on Computer Vision, pp 325–341
- Yu F, Koltun V (2016) Multi-scale context aggregation by dilated convolutions. In: International Conference on Learning Representations
- Yuan Y, Wang J (2018) Ocnet: Object context network for scene parsing. arXiv preprint
- Yuan Y, Chen X, Wang J (2020) Object-contextual representations for semantic segmentation. In: European Conference on Computer Vision, Springer, pp 173–190
- Zhang H, Cisse M, Dauphin YN, Lopez-Paz D (2017) mixup: Beyond empirical risk minimization. In: International Conference on Learning Representations
- Zhang L, Li X, Arnab A, Yang K, Tong Y, Torr PH (2019) Dual graph convolutional network for semantic segmentation. In: British Machine Vision Conference, p 254
- Zhang L, Xu D, Arnab A, Torr PH (2020) Dynamic graph message passing networks. In: IEEE Conference on Computer Vision and Pattern Recognition
- Zhang P, Dai X, Yang J, Xiao B, Yuan L, Zhang L, Gao J (2021a) Multi-scale vision longformer: A new vision transformer for high-resolution image encoding. In: IEEE International Conference on Computer Vision, pp 2998–3008
- Zhang Z, Zhang H, Zhao L, Chen T, Pfister T (2021b) Aggregating nested transformers. arXiv preprint
- Zhao H, Shi J, Qi X, Wang X, Jia J (2017) Pyramid scene parsing network. In: IEEE Conference on Computer Vision and Pattern Recognition, pp 2881–2890
- Zhao H, Zhang Y, Liu S, Shi J, Change Loy C, Lin D, Jia J (2018) Psanet: Point-wise spatial attention network for scene parsing. In: European Conference on Computer Vision, pp 267–283
- Zhao H, Jia J, Koltun V (2020) Exploring self-attention for image recognition. In: IEEE Conference on Computer Vision and Pattern Recognition
- Zheng S, Jayasumana S, Romera-Paredes B, Vineet V, Su Z, Du D, Huang C, Torr PHS (2015) Conditional random fields as recurrent neural networks. In: IEEE International Conference on Computer Vision, pp 1529–1537
- Zheng S, Lu J, Zhao H, Zhu X, Luo Z, Wang Y, Fu Y, Feng J, Xiang T, Torr PH, Zhang L (2021) Rethinking semantic segmentation from a sequence-to-sequence perspective with transformers. In: IEEE Conference on Computer Vision and Pattern Recognition, pp 6881–6890
- Zhou B, Zhao H, Puig X, Xiao T, Fidler S, Barriuso A, Torralba A (2019) Semantic understanding of scenes through the ade20k dataset. *International Journal of Computer Vision* 127:302–321